Politecnico di Torino

Master of Science in Energy and Nuclear Engineering

MASTER THESIS

Evaluation of the Radiosensitizing Capabilities of Target-Specific Gold Nanoparticles (AuNPs) in the Radiotherapy of Glioblastoma

Centro de Ciências e Tecnologias Nucleares (IST, Lisbon)

Candidate:
Antonella De Matteis

Supervisors:
Prof. Gianni Coppa
Dr. António R. Paulo (C^2TN/IST)
Dr. Fernanda M. Marques (C^2TN/IST)

Co-supervisor:
Dr. Salvatore Di Maria(C^2TN/IST)

Academic Year 2019/2020

Hic et nunc.

Abstract

The present dissertation, developed at Centro de Ciências e Tecnologias Nucleares (IST, Lisbon), intended to evaluate the irradiation effects of ^{60}Co beam source on gliobastoma multiforme cell lines in which gold nanoparticles (AuNPs) are dispersed. In order to study the effect of lower energy on AuNPs and compare results with ^{60}Co energy also a 50 kVp χ-ray beam was considered in this work. The major aim was to computationally investigate the dose enhancement effects (DEF) due to the gold used as radiosensitizer varying different parameters such as the cell size, the source beam and the location of the AuNPs in the nucleus or in the cytoplasm of the cell.
Towards this goal, the present work proposes to evaluate the dose enhancement factor in the nanometers and micrometers range surrounding the gold nanoparticles.
In the first part, the validation of the model is performed by evaluating the energy deposition and the DEF due to the AuNPs presence.
Secondly, a sensitivity study was performed for ^{60}Co and 50 kVp χ-ray irradiation in order to assess the effect, on energy deposition, of the lack of electronic equilibrium in the several irradiation setups.
Finally, based on previous experiments done on T98G cell line and on the validation and sensitivity study part, the concentration study is performed considering a constant cluster internalization of AuNPs of 30% located in the nucleus or cytoplasm for four different cell size.
The results show that the lack of electronic equilibrium could take to DEF overestimation that should be considered in modelling studies. Also, it is possible to maximize the dose enhancement factor in the first 100 nm around the AuNPs cluster located in the nucleus obtaining an average DEF of 1.96 and 152 for ^{60}Co and 50 kVp χ-ray respectively. Instead, for a cluster of AuNPs located in the cytoplasm the DEF decrease of one order of magnitude, respect the nucleus concentration, for 50 kVp χ-ray, with an almost linear shape for the MeV energy (i.e. ^{60}Co) whereas a DEF peak in the first 100 nm of nucleus and cytoplasm are detected using 50 kVp χ-ray source and with a rapid decrease in the micrometers range, seeming to reach an asymptotic value after the first micrometer.
In summary, the work described in this dissertation demonstrated and confirm the advantage of the use of gold nanoparticles as radiosentizers to enhance the dose delivered to cancer cells, and contribute to a preliminary definition of an irradiation strategy to follow in order to maximize the DEF. Coupling the simulation results with future experiments will be fundamental to understand the biological effect using different energy sources and with different AuNPs cluster concentrations.

Keywords: Gliobastoma, Gold nano-particles, AuNPs, radiotherapy.

Sommario

Questa tesi è stata sviluppata al Centro de Ciências e Tecnologias Nucleares (IST, Lisbon) con l'intento di valutare gli effetti radiologici derivanti dall'uso di nanoparticelle di oro (AuNPs) disperse in linee cellulari di gliobastoma, irradiate da ^{60}Co. È stata inoltre considerata una sorgente di 50 kVp emittente raggi χ, al fine di studiare e comparare gli effetti dovuti ad un'energia di sorgente minore di 1 MeV con quelli ottenuti da irragiamento con ^{60}Co. L'obiettivo principale è quello di indagare a livello computazionale gli effetti di un aumento della dose (DEF) causati dalla presenza di nanoparticelle oro, agenti come radiosensibilizzanti, variando alcuni parametri quali la dimensione cellulare, il tipo di sorgente e la localizzazione delle AuNPs nel nucleo o nel citoplasma. Lo scopo principale del lavoro è quello di valutare il dose enhancement factor nell'ordine dei nanometri e micrometri circostanti le nanoparticelle di oro.
Nella prima fase si è validato il modello, attraverso la valutazione dell'energia depositata e del DEF ottenuto in presenza di AuNPs, seguito da uno studio di sensibilità con sorgenti ^{60}Co e 50 kVp raggi χgrazie al quale si è osservata una sovrastima del DEF causato dal mancato equilibrio elettronico.
Infine, sulla base di precedenti esperimenti condotti sulla linea celluare T98G e dei risultati ottenuti nella fase di validazione e studio di sensibilità, si è eseguito uno studio di concentrazione con un'internalizzazione delle AuNPs costante e pari al 30% nel nucleo o citoplasma, considerando quattro diverse dimensioni cellulari.
I risultati ottenuti dimostrano che la mancanza di equilibrio elettronico potrebbe indurre ad una sovrastima del DEF che dovrebe, quindi, essere considerata negli studi di modelizzazione. È possibile, inoltre, massimizare il dose enhancement factor nei primi 100 nm attorno alle AuNPs situate nel nucleo ottenendo un DEF medio di 1.96 e 152 rispettivamente per ^{60}Co e 50 kVp raggi χ.
Se la concentrazione di AuNPs è localizzata nel citoplasma, la diminuizione del DEF risulta essere di un ordine grandezza rispetto ad una concentrazione di AuNPs localizzata esclusivamente nel nucleo, per una sorgente di 50 kVp raggi χ. Mentre per sorgente ^{60}Co il DEF risulta avere un adamento piuttosto lineare.
Una peculiatità della configurazione con concentrazione 0%-100% nucleo-citoplasma, viene rilevata con sorgente 50 kVp raggi χpoichè si evidenzia un picco del DEF nei primi 100 nm nel nucleo e nel citoplasma seguito da una rapida riduzione nel range dei micrometri, fino a sembrar raggiungere un valore asintotico dopo il primo micrometro.
In sintesi, il lavoro descritto, ha dimostrato e confermato il vantaggio dell'uso di nanoparticelle di oro che utilizzate come radiosensitivizzanti postrebbero aumplificare la dose somministrata alle cellule tumorali e contribuire alla definzione perliminare di una strategia di irradiazione per ottenere una massimizzazione del DEF.
L'associazione dei risultati ottenuti dalle simulazioni con futuri esperimenti di applicazioni

sulle linee cellulari di gliobastoma sarà fondamentale per comprendere l'effetto biologico derivante dall'utilizzo delle AuNPs, utilizzando diverse sorgenti di irraggiamento e diverse concentrazioni.

Acknowledgements

First of all I would like to thank to Prof. Gianni Coppa (Politecnico di Torino) for its moral and academic support from Italy to the development of this project during the Covid-19 period, nobody would have imagined the outbreak of a pandemia.

My huge thanks goes to my supervisors António Rocha Paulo and Fernanda Marujo Marques (C^2TN/IST) for all their advice and help with the thesis. I am infinitely grateful for their support, patience and availability during these months.

I also would like to thank to my co-supervisor, Salvatore Di Maria, for his fundamental support providing me good advice in the development of the model used for the thesis.

Thanks to Ana for her collaboration and exchange of knowledge, always ready for brainstorming.

Finally, I would like to thank all people met at C^2TN, thanks for the time spend with me trying to learn Portuguese at lunch time and coffee break. I am thankful for all the assistance and companionship provided.

Contents

List of Figures

List of Tables

List of Abbreviations

CLDR	Continuos low-dose Rate
CNS	Central nervous System
C^{2}TN	Centro de Ciências e Tecnologias Nucleares do Técnico
DEF	Dose enhancement factor
DNA	DeoxyriboNucleic acid
DSB	Double strand break
EGTR	Epidermial growth factor receptor
EPR	Enahnced permeability and retention
GBM	Gliobastoma multiforme
HDR	High dose rate
IR	Ionizing radiation
IST	Instituto Superior Técnico
LDR	Low dose rate
LET	Linear energy transfer
LINAC	Linear accelerator
LQM	Linear quadratic model
MC	Monte Carlo
MDR	Moderate dose tate
NK-1	Neurokinin-1 receptor
NP	Nanoparticles
NTCP	Normal tissue complication
PDR	Pulsed dose-rate
RBE	Relative biological effectiveness parameter
RNA	Ribonucleic acid
ROS	Reactive oxygen species
SSB	Single strand break
TC	Tumor control
TCP	Tumor control probability
TEM	Transmission electron microscopy
WHO	World Health Organization

List of Symbols

Ag	Silver
Au	Gold
cGy	Centigray (cGy = 0,01 Gy)
e^-	Electron particle
Gd	Gadolinium
H_2O	Dihydrogen Monoxide (water)
H_2O^+	Oxoniumyl water ion
H_3O^+	Hydronium ion
^{125}I	a radioisotope of iodine with half-life of about 59 days
^{103}Pd	a radioisotope of palladium with half-life of about 17 days
kVp	Kilovolt peak (in x-ray tubes)
MeV	Megaeletron volt (unit of energy: 10×10^6 eV)
mM	Millimolar (corresponding to 10^{-3} mol/L)
OH^-	Hydroxyl radical
Z	Atomic number

Chapter 1

Introduction

An irregular growth of cells is a characteristic hallmark of the cancer. The growth of these cells can lead to different consequences depending on the location, dimensions and associated grade. The brain tumor, in particular Gliobastoma, is considered one of the most severe tumor due to its location, penetration, several consequences associated and its removal difficulty and radiotherapy resistance. In the Introduction some biological and physical fundamentals are briefly described, trying to answer to the following questions:

- what is cancer?
- How can it be treated?
- What is the physic hidden in radiotherapy?
- What are the biological effect of radiotherapy?
- What does it mean radiosensitizers?
- what is Gliobastoma?

The chapter ends with the description of the aim and the motivation of the performed analysis for the valuation of the Dose Enhancement Factor.

1.1 Cancer: Definition and Incidence

Cancer is the major global health burden. It is considered the first cause of death in economically developed countries and the second cause in developing countries.[14] The WHO estimates that it is one of the leading causes of death after heart diseases, stroke and respiratory infections. Despite the increase of the technological progress some unhealthy lifestyle factors as tobacco consumption, air pollution, inadequate nutrition, physical inactivity and harmful use of alcohol contribute to the risk of cancer occurrence.[36] In addition some biological factors as mutations, immune conditions, and hormones imbalances can lead to the origin and the advancement of cancer.(Figure 1.1)

Cancer diseases consist into an irregular growth of cells due to different changes in genoma expression leading to an evasion from the regular apoptosis. This mechanism allows to the creation of a new population of cells that can penetrate in different tissues causing morbidity and in the worst case the death of the host.[14][49]

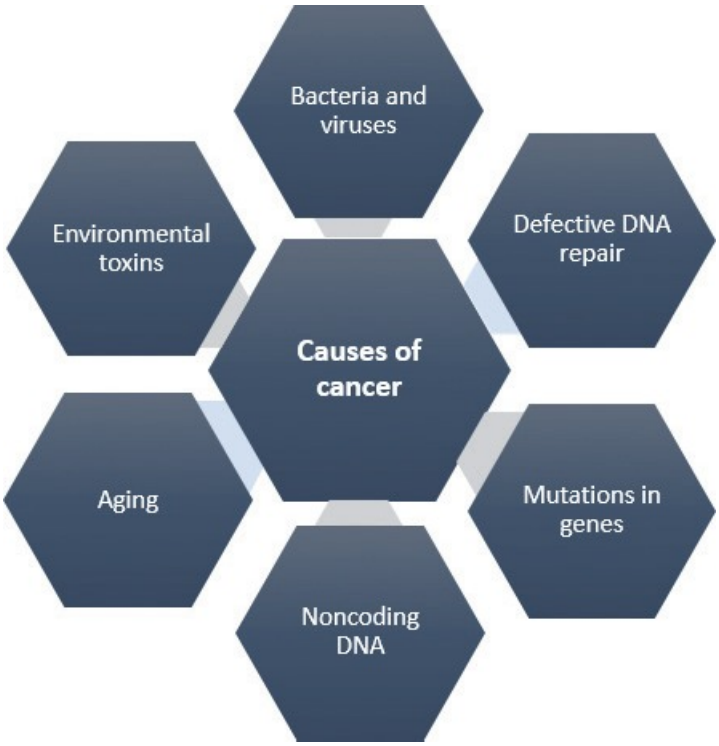

Figure 1.1: Causes of cancer. [2]

Cancer cells appear having irregular patterns and morphology compared to the healthy cells. They can be smaller or sometimes larger and their nucleus appear larger and darker than normal cells. Moreover, cancer cells can originate a cancer metastasis if they spread to tissues and organs beyond where the tumor originated. Tumors can be classified considering the type of tissue in which they originate (histological type), as exemplified below:

- Carcinoma, in epithelial tissue;
- Sarcomas, in connective tissue;
- Leukemia, in blood cells;
- Osteosarcoma, in bone marrow.

However, despite the common affected body area, the biological, geometrical and local characteristics of each tumor differ. For this reason, the methodologies to treat cancer vary and sometimes are used in a combined way.

1.2 Cancer Treatment Modalities

Surgery, chemotherapy and radiation therapy represent the conventional modalities to treat cancer, while immunotherapy has become a standard treatment only in the past two decades. Generally, surgery or radiation therapy represent the primary treatments, which are often complemented with an adjuvant and/or neoadjuvant therapy as chemotherapy or immunotherapy. In particular, the neoadjuvant treatment helps to shrink the tumor before the main treatment while the adjuvant effects kill undesirable tumor cells left behind.[14] The mainly treatment modalities are shown in Figure 1.2.

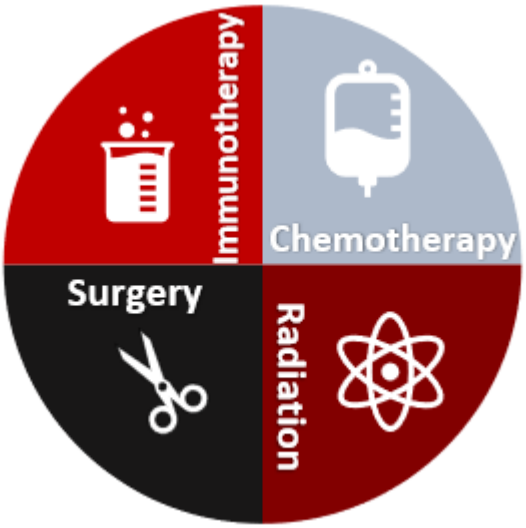

Figure 1.2: Main cancer treatment modalities.

1.2.1 Surgery

Surgery is the oldest and most recurrent treatment.[54] The procedure is invasive and requires cuts through skin, muscles and sometimes bones that can take a long time to recover form. Due to the localized action the damage to the surrounding tissues is lower compared to chemotherapy and radiation therapy, it can be used to:

- remove localized tumor and isolated metastasis especially if the disease is early diagnosed;
- debulk a tumor, removing a part of the tumor in order to optimize other treatments;
- alleviate cancer symptoms like pain or pressure.

Surgery has a limited role in treatment for disseminated cancers like leukemia. The main reason is that the cancer cells usually spread throughout the body as the blood circulates. Because leukemia is a systematic condition, the best treatment approach is usually chemotherapy or immunotherapy.

After treatment, pain is probably the most common complaint of surgery patients but other complications can occur such as infections like pneumonia. Moreover, cancer is most

likely to come back because some cancer cells were left behind during the surgery. For this reason extra treatments are necessary aiming to try to control or kill any cancer cells left. Innovations in surgery have improved not only the instruments used to cut tissue and extract tumor mass, but, importantly, the oncological outcomes and the patient life quality. Thanks to the awareness of the growth patterns and invasion, specific local approaches are possible where often surgery and radiation are the most successful treatment for localized tumors. [42][54][2]

1.2.2 Chemotherapy

Chemotherapy is a therapeutic modality that uses chemical drugs to destroy cancer cells in the body. It is considered a systemic treatment, which means it affects the entire body and can cause serious side effects that can severely impact the quality of life of the patient. Often it is used in combination with other therapies, such as surgery, radiation, or hormone therapy. However, the choice of this therapeutic modality depends on:

- the stage and type of cancer;
- the previous cancer treatments;
- the location of the tumor;

There are more than hundred known drugs used alone or in combination with other therapies with different chemical structure and composition. For example, alkylating agents, as cisplatin, act stopping the cancer cell division damaging the DNA and antimetabolites agents, as fluorouracil and methotrexate, stop the DNA synthesis and RNA growth. This kind of treatment requires multiple cycles and different sessions interspersed by break periods, or in combination with other therapies to be effective.
However, drugs also affect normal cells leads to side effects such as fatigue, nausea, hair loss, vomiting and infections due to induced immunodeficiency or even death in the worst cases. [2][42][54]

1.2.3 Immunotherapy

Immunotherapy is a biological type of cancer treatment that helps the immune system to fight cancer using substances made from living organisms. It is a systematic therapy based on the action of the immune system, normally using antibodies that bind to proteins expressed by cancer cells, inhibiting their function.[54]
Normally, the immune system is able to detect and kill abnormal cells but cancer cells escape thanks to genetic changes or expression of proteins on their surface i.e., the immune system do not recognize them as abnormal. Due to the complex interaction between tumors and immune cells, often combination therapy is used to generate protective antitumor immunity.[8] This kind of treatment requires different cycles of different duration based on the type of cancer.
Depending on the type of immunotherapy received some side effects may occur, especially when the immune system also acts against healthy cells and tissues. The most common are skin reactions like pain and swelling or flu-like symptoms like fever, fatigue, nausea and other effects.[42]

1.2.4 Radiation Therapy

After the discovery of the X-rays by Wilhelm Conrad Röntgen in 1895, the role of ionizing radiation (IR) immediately originated an immense interest in the public and also initiated intense research in several directions, in particular radiology. However, only in the late 19^{th} century radiation therapy becomes a recognized medical speciality, thanks to Marie Curie winner of the Nobel prize for her studies in radioactive elements. She discovered polonium and radium and studied its radioactive properties, its effects on biological tissues and the capability to destroy cancer cells.[50] Radioactive compounds became important as sources of radiation in both scientific experiments and in the field of medical applications.
The radiation therapy, also called radiotherapy, is a localized, non-invasive treatment based on the use of radiation to kill and shrink tumors. The DNA of tumor cells is damaged by high energy radiations, which slow or stop the cell division and their ability to proliferate. It is used to:

- shrink tumor, if done before surgery;
- kill remaining cancer cells after surgery;
- reduce the cancer relapse.

The treatment, generally, requires several days or weeks to make tumor cells die. During this period genetic damage occurs also for adjacent healthy cells causing side effects as fatigue. Other radiation side effects as hair loss and skin changes occur depending on the part of the body affected.[42][2]
Over 50% of cancers are treated by radiation therapy. Thanks to the combined use of imaging techniques, computerized treatment planning systems and radiation treatment machines, in rapid progress, there is a continuous improving of the therapeutic outcomes and better understanding of the radio-biological effects.[14]
The common cancers treated with radiotherapy are shown in the Table 1.1.
The goal of radiotherapy is to optimize the radiation beam in order to deliver energy only in the cancer cells, minimizing the energy delivered in the adjacent healthy cells.
The external beam therapy, brachytherapy or internal beam therapy, are the main approaches to deliver radiation in the body. (Figure 1.3)[43]
Both of them can be classified considering the delivered dose rate defined as the absorbed radiation into material) as [38]:

- Low dose rate (LDR): from 40 to 200 cGy per hour;
- Moderate dose rate (MDR): from 200 to 1200 cGy per hour;
- High dose rate (HDR): from 1200 cGy per hour;

External beam therapy, in fact, has limitations regarding the location of the device and the cost of constructions and maintenance due to the power supply required. However, brachytherapy is not appropriate in case of a wider field irradiation request. Both modalities are discussed below in more detail.

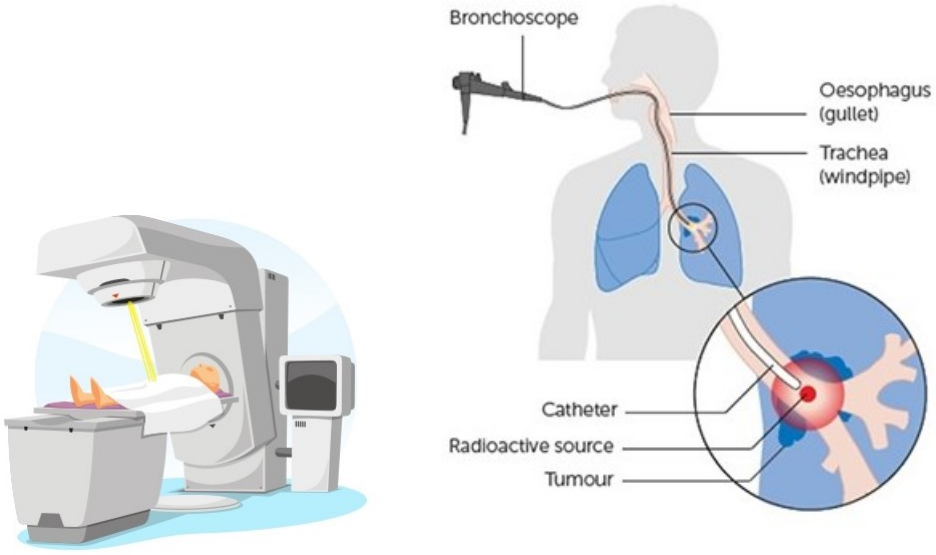

(a) External Beam Therapy **(b)** Brachytherapy

Figure 1.3: Main radiation therapies. [40]

External Beam Therapy

The use of an external source to deliver energy is called external beam therapy. High energy rays as photons, protons or other particle radiations are directed from equipment to the tumor region. The use of photons is the most conventional clinical treatment.[14][44] Table 1.2 shows the equipment used to create determined energy photons to treat tumors considering their depth.
The radiation produced by the units listed in the Table 1.2 are called χ-rays except for that produced by ^{60}Co that is called γ-rays. This type of radiation was used in the Gamma Knife model invented by Lars Leksell in 1968, a treatment that is still used today to cure brain tumors and vascular malformations. Its advantage lie in the efficiency, precision and reliability to deliver radiation in the tumor area, and the ease of use/maintenance.[39]
Neutrons, pions and heavy ions beams, like carbon, neon and argon, are produced in cyclotrons and synchrotron units. These particles beams, compared to photons, cause a higher damage on healthy cells because they deposit more energy along their path. Proton beams, also generated in cyclotrons and synchrotrons, are being studied for cancer therapy because they can allow a better dose distribution and less toxic effect compared to photons.[48] The overall dose of radiation given to the healthy tissue in proton beam therapy is lower than with conventional radiotherapy, a desirable feature when weighing the potential risks. The common way to administering external radiation therapy is called fractionation. It allows the delivery of high total dose to tumor administering it in multiple doses

Table 1.1: List of common cancers treated with radiation therapy [14]

Early cancers curable with only radiotherapy	Cancers curable with radiotherapy combined with other therapies
Skin cancers	Breast carcinomas
Prostate carcinomas	Rectal and anal carcinomas
Lung carcinomas (non-small cell)	Local advanced cervix carcinomas
Cervix	Locally advanced head and neck carcinomas
Lymphomas (Hodgkin's and low-grade Non-Hodgkin's)	Locally advanced lung carcinomas
Head and neck carcinomas	Advanced lymphomas
	Bladder carcinomas
	Endometrial carcinomas
	CNS tumors
	Soft tissue sarcomas

Table 1.2: Examples of tumour treatment facilities: photons energy generated, maximum body depth achieved.[48]

Unit Name	Photon Energy	Tumor Depth [cm]
Superficial therapy unit	50 - 100 [kVp]	0
Orthovoltage therapy unit	100 - 300 [kVp]	0.5
Cobalt-60	1173 and 1.332 [MeV]	1.5
Linear accelerator(LINAC)	6 [MeV]	1.5
LINAC	10 [MeV]	2.5
LINAC	22 [MeV]	4

Brachytherapy

Brachytherapy can be considered as the radiation therapy that acts from inside the body. It means that the radiation is delivered by a sealed radioactive source, as ^{125}I or ^{103}Pd, into the tumor site. Its position varies with the type of cancer: it is interstitially placed in case of breast and prostate cancer, on the surface for skin tumor or intracavitary for cervical cancer. Compared to the external beam, the brachytherapy allows a potential reduction of the dose received by normal tissue because radiation does not pass through skin tissue or other organs to reach tumor. So, the most energy delivered is near its location. The principal way to deliver energy in brachytherapy is continuous low dose-rate (CLDR) but a pulsed dose-rate (PDR) is also used with the advantage of a better dose optimization. [44][43][48]

1.3 Radiation-matter interaction

Ionizing radiations (IR) consists of charged particles radiations and neutral radiations including photons. One important difference between the IR consists in the way they cause ionization. In fact, while charged particles cause directly ionizations passing through the matter, neutral radiation (photons and neutrons) transfer their energy to an energetic light charged particle that in its turn cause indirectly ionizations. The energy of uncharged particles is only partially transferred to a charged particle, being the remaining part delivered as radiation, i.e. photons. Interaction with matter depends on the type of charged particles but it is also influenced by the energy of the particle beam and the target material properties.[46][48]

1.3.1 Photon and charged particle interactions

The photon-matter interactions can involve both the nucleus and orbital electrons. The main physical interactions, shown in Figure 1.4, are:

- Compton scattering, due to the interaction with the photon and a loosely bound electron;
- Photoelectric effect and Rayleigh effect, due to the interaction between the photon and a bound electron;
- Pair production, due to the interactions between the photon and the electrostatic field of the nucleus.

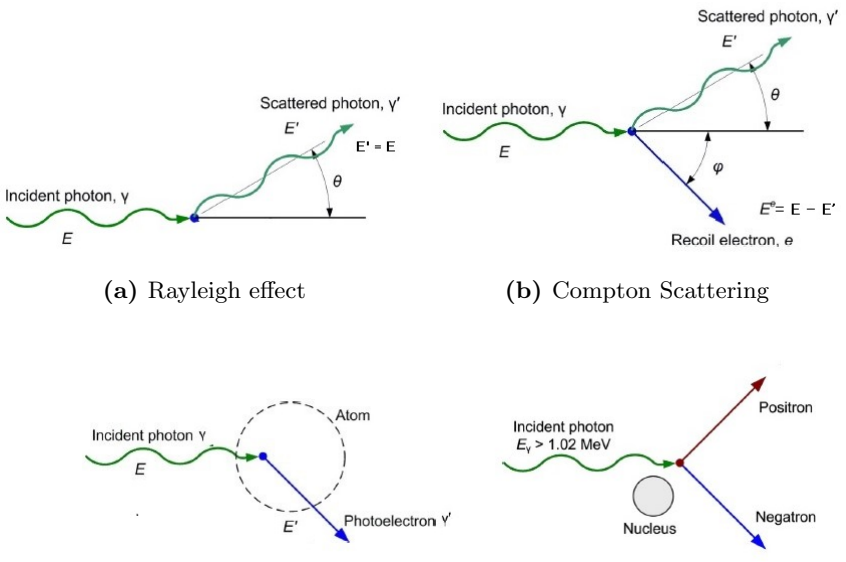

(a) Rayleigh effect **(b)** Compton Scattering

(c) photoelectric Effect **(d)** Pair Production

Figure 1.4: Schematic representation of the main interactions with photons in matter, where (a) corresponds to the Rayleigh effect, (b) to the Compton scattering, (c) to the Photoelectric effect, (d) to the pair production. Adapted from [46]

As stated before, photon beams are not directly involved in ionization events. The primary event is the transference of energy to the matter. If this energy is able to remove an electron from its orbital, an ionization event occurs so the atom becomes ionized. If it is not the case, the electron passes to a more energetic orbital and the atom becomes excited.[46] By contrast, electrons are charged particles causing excitation or direct ionization in the matter due to continuous Coulomb interactions. In particular, fast electrons are involved in inelastic orbital collision able to ionize and excite the matter or generate photons through bremsstrahlung emission. (Figure 1.5)

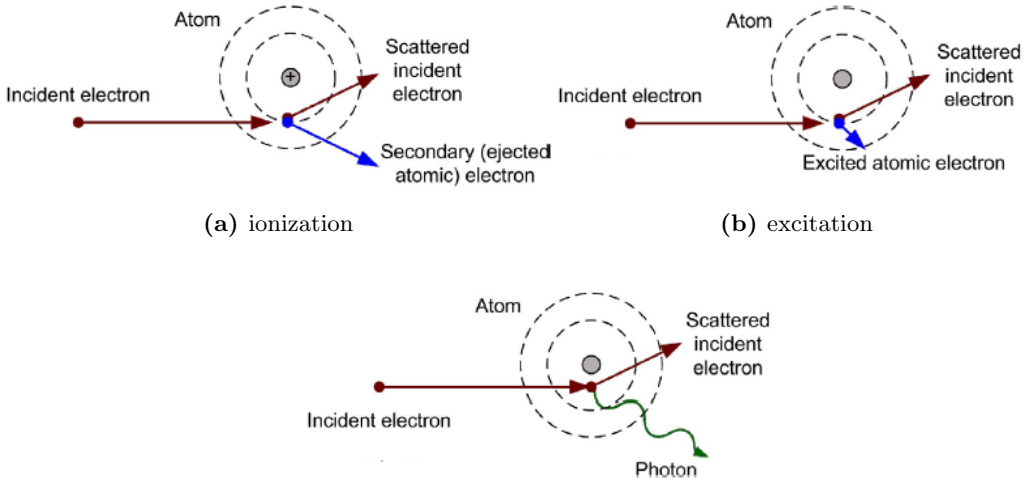

(a) ionization

(b) excitation

(c) bremsstrahlung

Figure 1.5: Schematic representation of the main interactions with electron in matter, where (a) corresponds to the Ionization, (b) to the Excitation, (c) to the Bremsstrahlung. Adapted from [46].

Absorbed dose and Linear Energy Transfer (LET)

The absorbed (D) dose is the principal metric quantity used in radiation therapy to plane, prescribe and deliver the radiation treatment. It is defined as the amount of energy (ΔE) transferred to the exposed material mass (Δm) and represent the mean energy deposited by IR into matter during its path:

$$D = \frac{\Delta E}{\Delta m} \quad [Gy] \tag{1.1}$$

Where
1 Gy = 1 J kg^{-1}.[46]

The Linear Energy Transfer (LET) is the microscopic metric quantity used to characterised the quality of an IR. It is defined as the average energy (dE) that a charged particle transfers to the medium in an small distance (dl).

$$LET = \frac{dE}{dl} \quad [\frac{keV}{\mu m}] \tag{1.2}$$

LET can be distinguished into low-LET and high-LET depending on the ionization density. Low-LET radiations are associated to χ-ray or γ-ray and they are sparsely ionizing i.e. photons can travel along the molecules without depositing their energy. High-LET radiations are generated from heavy charged particles and defined as densely ionizing radiation because they deposit most of the dose near the particle track. Due to the ionization density, high-LET radiations are considered biologically more effective to produce DNA damage when compared with low-LET radiations. The cell response to different radiation qualities is measured by the relative biological effectiveness parameter (RBE). RBE is defined as the fraction between the dose of the reference radiation and the dose of the test radiation used to give the same biological effect. Usually, the references low-LET radiations considered are the 250 kVp χ-rays and the ^{60}Co γ-rays, due to their easy availability.[44] The cell response is hence related to the particle energy and its LET. For a given particle when its energy increases the LET decreases and consequently the biological effectiveness decreases. For example, χ-rays and γ-rays both generate secondary fast electrons but a 1.1 MeV cobalt-60 γ-photon has lower LET than 250 kV χ-rays and consequently a biological effectiveness of about 10% less. (Table 1.3)[9]

Table 1.3: Typical LET values for different low LET radiation beams and high LET radiation beams. Generally ,10 eV/µm LET is considered to separate high-LET radiations from low-LET radiations.[48]

Low-LET radiation	LET [keV/µm]	High-LET radiation	LET [keV/µm]
X-rays : 250 kVp	2	Electrons: 1 keV	12.3
γ-rays: Co-60	0.3	Neutrons: 14 MeV	12
X-rays: 3 MeV	0.3	Protons: 2 MeV	17
Electrons: 10 keV	2.3	Carbon ions: 100 MeV	160
Electrons: 1 MeV	0.25	Heavy ions:	100 - 2000

Generally, LET of about 100 keV/µm provides the most effective biological effects because it allows ionization events with spatial density of about 2 nm which is equivalent to the

diameter of DNA strand. Nevertheless, this value changes with different cell types, spectrum of LET values in the radiation beam and mean LET.[44]

1.3.2 Mass attenuation coefficient

Another important parameter is the total mass attenuation coefficient (μ/ρ) connecting the photon or particle which gives an idea of how easy is the penetration of a beam in a certain media. The word 'mass' identify the material density (ρ) in which the beam passes through while the 'total attenuation coefficient' (μ) suggests that this parameter comes out from a sum, in particular it is defined as the sum of the attenuation coefficients of all interactions happening. For photon-matter interactions the attenuation coefficient is given by the following equation, which accounts for the different probability of given photon-matter interactions:

$$\mu = \tau + \sigma_R + \sigma_C + k_i \quad [\frac{1}{cm}] \tag{1.3}$$

where:

- $\tau$is the photoelectric attenuation coefficient;
- σ_R is the Rayleigh scattering attenuation coefficient;
- σ_C is the Compton effect attenuation coefficient;
- k_i is the pair production attenuation coefficient.

Consequently, the total mass attenuation coefficient is given by the ratio of the total attenuation coefficient to the density of the absorber media (μ/ρ). The mass attenuation coefficient depends on the photon energy and on the atomic number of the media.
Figure 1.6 shows that, in water, for low photon energies, the major contribution to the total mass attenuation coefficient is due to the photoelectric and Rayleigh effect. The Compton effect is dominant in the energy interval range of 20 keV - 30 MeV while pair production become dominant only for photon energy higher than 30 Mev. [48] The human cell consists approximately of 70% water. So, the values of the attenuation factors in water can be considered almost equivalent to those in soft tissue.

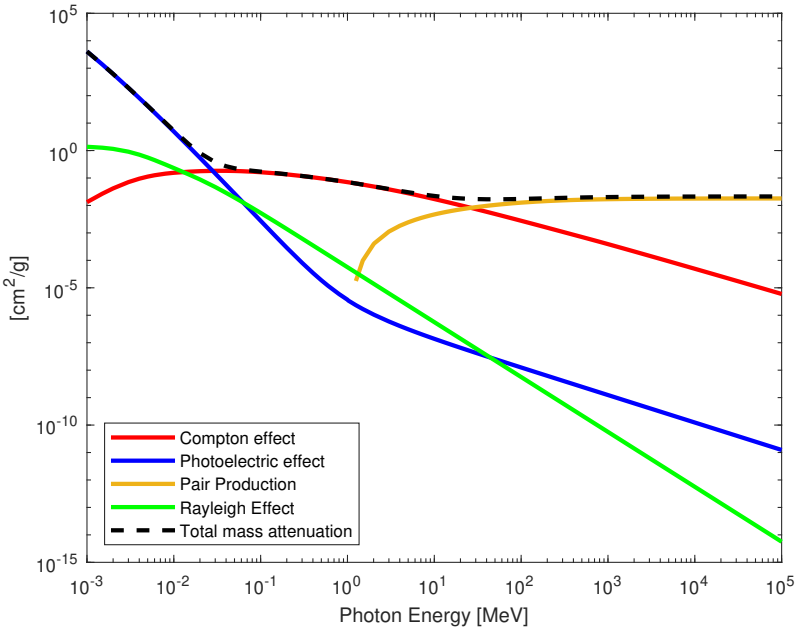

Figure 1.6: Mass attenuation coefficients in water as function of photon energy (values taken from the NIST XCOM database) [47]

1.4 Mass energy absorption coefficient

Directly related to the mass energy coefficient is the mass energy absorption coefficient (μ_{en}) defined as the mean energy transferred from the secondary charged particles to the absorber ($\overline{E_{en}}$) multiplied by the mass attenuation coefficient (μ/ρ) and divided by the photon energy ($h\upsilon$).

$$\frac{\mu_{en}}{\rho} = \frac{\mu}{\rho}\frac{\overline{E_{en}}}{h\upsilon} \quad [\frac{cm^2}{g}] \tag{1.4}$$

The mass energy absorption coefficients depends on the photon energy and on the atomic number of the media. [48]

1.5 Biological effects of radiation

The clinical relevance of radiotherapy relies on the biological effects of IR on target cells. The cellular damage involves three main phases in which, starting from the photon beam and passing by chemical reactions, the damage of the DNA is developed. The first phase of this process is the physical one. It starts with the irradiation and involves both direct and indirect ionization events. An absorbed dose of 1 Gy is able to generate more than one hundred thousand cell ionizations. After the ionization events, breakage of molecular bonds and a cascade of chemical reactions occurs. This is the so-called chemical phase in which free radicals react with the surrounding matter. These physical and chemical phases are the shortest, taking less than a second to occur and continuing until photons and particles lose their energy. The last phase occurs when DNA is damaged. It can take seconds, days or years

considering the dose, the number of treatment and the cells reaction. The damage to DNA can occur directly with the breakdown of the molecular connection or indirectly due to free radicals formed in the chemical phase, this last phase is the biological one and involves the response to IR at molecular, cellular and tissue level.(Figure 1.7) [44][6][28]

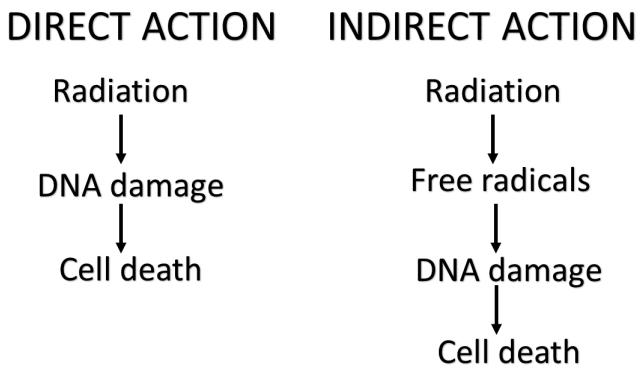

Figure 1.7: Direct and Indirect effects of radiations.

1.5.1 DNA damage

IR causes indirect damage due to free radicals, reactive oxygen species (ROS) produced close to DNA during the chemical phase. The composition of cells is made of water (about 70%), so the free radicals produced are the hydroxyl radicals coming from the ionization of the water:

1. the water molecule (H_2O) is ionized generating an oxoniumyl water ion ($H20^+$) and an electron (e^-);
2. the water ion reacts with water molecule generating an hydronium ion (H_3O^+) and an hydroxyl radical (OH).

$$\begin{aligned} H_2O &\longrightarrow H_2O^+ + e^- \\ H_2O^+ + H_2O &\longrightarrow H_3O^+ + OH^- \end{aligned} \tag{1.5}$$

The rupture of molecular bonds and the oxidation of DNA are direct consequence to the radicals generation, while secondary electrons produced can lead to DNA strand breaks. Strand breaks are classified in single strand break (SSB) and the double strand break (DSB) (Figure 1.8). SSBs consist in one or more breaks of single DNA strand. These injuries have not relevant biological consequences because they are quickly repaired using the second strand as template. They normally occur in the cell, for example during cell replication, and can lead to mutation in case of incorrect reparation. However, more SSBs or frequently lesions, for example base lesion, in the same strand at short distance between them, can generate clusters less reparable, often leading to an increase in mutation rates. More important biological effects are due to DSBs. These damages are less frequent than SSBs, nonetheless, they can involve the lost of the genetic information. DSBs may originated from:

- two SSBs in opposite strands;
- two SSBs no-time correlated;
- two induced SSBs with the same primary event.

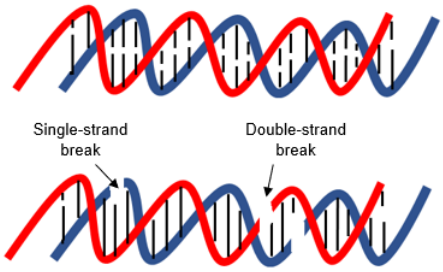

Figure 1.8: Representation of DNA breaks: SSB and DSB.

As said before, a delivered dose of 1 Gy leads to more than one hundred thousand ionizations, 10^5, which is equivalent to about thousand SSBs and to twenty/forty DSBs. It follows that clusters formation and DSB damage have a strong contribution to cell death.[44]

1.5.2 Mechanisms of cell death

Healthy cell life is normally regulated by death mechanisms of apoptosis, necrosis and autophagy. In a tumor cell these processes are still responsible of cell death but can be altered. In addition, after radiation treatments, mitotic catastrophe and bystander signalling can also play a role in the induced cell death.

Apoptosis

Apoptosis is a form of programmed cell death occurring in different physiological processes as the embryonic development, the immune system operation and the homeostasis maintenance. It is characterised by a sequence of morphological events among which the condensation of chromatin on nuclear membrane and the nuclear fragmentation are the hallmarks. In cancer cells the alteration of the programmed death leads to its proliferation. However, IR can induce the death of cancer cells by apoptosis. [9][44]

Necrosis

In contrast to apoptosis, necrosis is an induced cell death, also defined as 'death by injury', occurring in unfavourable conditions as energy loss and ion imbalance where the cell damage make the cell unable to function. Cellular swelling and membrane deformations are characteristics signs of this mechanism occurring after an infection. Radiation treatments, damaging the DNA, can induced necrosis with different frequencies associated to different kind of cells.[9][44]

Autophagy

Autophagy is not properly a mechanism of cell death but it is associated to the digestive cell procedure to generate macro-molecules and energy, recycling their own cytoplasm content with the aim to ensure the homeostasis. However, in radiotherapy autophagy alone is induced both in healthy and cancer cell leading to about the 20% of cell death. Despite this evidence, the role of autophagy after irradiation can be twofold: it could increase the radiation efficiency through endoplasmic reticulum stress or benefit tumour cells ensuring homeostasis.[52][9][44]

Mitotic death

The mitotic death occurs as often as apoptosis in most tumor and sometimes it represents the only cell death modality. The damage to chromosomes is the primary event causing the cell kill meanwhile the first or second dividing process is attempt to create a new generation. A mitotic catastrophe occurs if the chromosome damage is severe enough to complete prevent the mitosis or to activate other forms of cell death.[9][44]

Bystander signalling

Bystander signalling involves biological consequences on cells not directly effected by radiation located close to the effected ones. Chromosomal aberrations, mutation and alteration of gene expression are some of the biological effects occurring with the bystander signalling. This effect is particularly important at low doses when an irradiated cell release factors in the medium through protein channels between cells resulting in indirect killing of non-target cells.[9]

1.5.3 Cell survival: Clonogenic assay

The clonogenic assay is an in vitro cell survival assay that consists in testing the ability of a single cell to produce a colony after a treatment with ionizing radiation. The same number of tumor cells are growth separately in the same culture medium. Then, one of these cell cultures are irradiated and others are used as non-irradiated controls. At least fifty cells are necessary to have a colony, this number correspond to five-six generations of cells and it is considered to exclude cells with a limited growth level. After a certain incubation time the colonies are fixed, stained and counted using a microscope. The survival fraction of cells is calculated as the ratio between plating efficiency of treated cells and the plating efficiency of non-treated cells. This value is often expressed in percentage and must be corrected considering the efficiency in the undamaged cells detection and the number of cells plated.[9][44] The connection between the clonogenicity and the radiation dose can be established using the linear quadratic model (LQM). This model allows to correlate the fraction of surviving cells (S) at a certain dose (D) describing the probability occurrence of lethal events due to a DSB from a single particle (α) or from two or more particles (β):

$$S = exp(-\alpha D + \beta D^2) \tag{1.6}$$

This is the most used model for the calculation of radiotherapy dose effects in different fractionation schemes.

The advantages of this model can be synthesized as follow:

- it is a mechanistic model based on biology;
- the few parameters involved are useful and practical;
- large part of other models predict the same fractionation dependencies;
- the effects of fraccionation predicted by the model are well verified in laboratory;
- it is good validated until 10 Gy/fraction and should be used up to 18 Gy/fraction.[5]

1.6 Radiosensitization and Radiosensitizers

The therapeutic window in which is possible to treat a tumor by radiotherapy is defined by the tumor control probability (TCP) and the normal tissue complication probability (NTCP). This window can be visualized as the space between the two probability curves that allows the minimization of adverse effects to the normal tissues and a good control of tumor irradiation. Graphically, TCP and NTCP can be represented as two sigmoid curves in which there is a sharp dose-response for intermediate doses and a low response for very high or very low doses. (Figure 1.9)

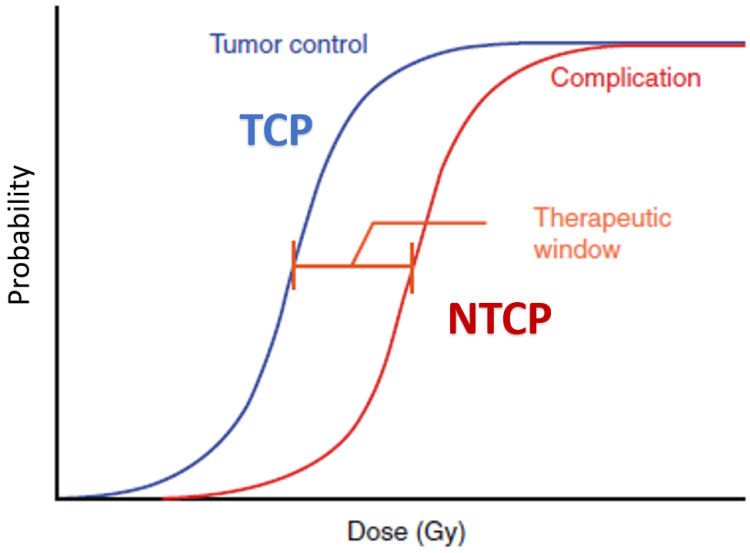

Figure 1.9: The therapeutic window as the difference between the TCP curve and the NTCP curve. Adapted from David et al. (2014). [33]

The tumor control probability is influenced by factors such as the individual tumor sensitivity, the clinical stage of the tumor and the total delivered dose. Theoretically, by increasing the dose delivered to tumor cells it is possible to obtain a good TCP. However, the NTCP drastically decreases with augmented toxicity to the close normal tissues that limits the amount of dose delivered. The window therapy shrinks for extended treatments and, in addition, some patients have radioresistance that makes the therapy less effective. Some specific tumors like

breast cancer, bladder cancer and glioblastoma are radioresistant to treatment because of intrinsic cancer cell radioresistance.[12][33] The effects of radiotherapy are strongly influenced by the oxidation level and so the hypoxic level due to the oxidation stress. Hypoxic cells are radioresistant during radiotherapy about three times more than well oxygenated cells.[34] Sometimes, the hypoxic level in tumor cells is higher than in healthy cells. Radiosensitization might be the therapeutic intervention to radiosensitize the tumor. In particular, high-Z materials are the most common radiosensitiezers used and studied due to their favourable properties.[1]

1.6.1 Chemical Radiosensitizers

Hypoxic regions contribute to a low response of tumor cells to IR. Therefore to increase the oxygen concentration during irradiation should be the easiest way to solve this problem.[34] However the administration of molecular oxygen alone to tumor cells is not easily feasible neither effective because of its rapid metabolization. Another direct way to reduce hypoxia consists in the use of hyperbaric oxygen, but this solution may increase the clinical complications. Stronger benefits are possible if a chemical agent with high electron affinity is administered in combination with carbogen breathing (95% oxygen, 5% carbon dioxide). However, the toxicity to normal cells also increases. Several compounds with low toxicity, in particular nimorazole, have been tested as radiosensitizers in brain tumor but the success was limited to a no-relevant increase of the lethal radiation effect. Other chemical agents with high electron affinity and low toxicity have also been considered. [44][22]

1.6.2 High-Z Radiosensitizers/Gold Nanoparticles

Another way to modulate the response to IR, focusing the radiation damage in the tumor cells can be obtained by nanostructures of metals with high atomic number. In particular, noble metals increase the efficiency of radiotherapy in the local site because of their physical and chemical properties. The cell damage is increased thanks to the electrons emitted by the action of IR that induces the inner shell ionization of metal atoms, combined with Auger electrons, emitted from the metal-based nanoparticles. The electrons produced are able to produce ROS. Some of the high-Z metals that have been studied are: gold (Z=79), silver (Z=47) and gadolinium (Z=64). It has been demonstrated that gadolinium (Gd), in particular metallotexaphyrin (Motexafin Gadolinio) can increase the generation of ROS and act as radiosensitizer. However, the in vivo release of Gd implies some toxicity issues namely nephrotoxicity. Silver (Ag) nanoparticles are able to induce apoptosis and produce ROS, due to its good radiosensitizing capability for radiotherapy. Gold nanoparticles (AuNP) can be considered the best metal-based nanoparticles to be used as radiosensitizers in radiation therapy because of its biocompatibility (higher than Ag) and inert state. Moreover, Au has an atomic number higher than Ag and Gd which can be an advantage. In fact, the energy produced by the photoelectric effect and the amount of secondary particles increase for higher atomic numbers.[37] [22]
Gold nanoparticles can be easily synthesised through chemical reductions methods and have other several advantages that make them suitble for the role of radiosensitizers.
AuNPs are rapidly eliminated from the body via urinary or hepatobilary system and present usually low toxicity. Due to their dimensions, some AuNPs might undergo the so-called enhanced permeability and retention (EPR) effect in the tumour tissues. Moreover, using

different chemical strategies, nanoparticles can be functionalized with a variety of ligands such as biomolecules or cytotoxic drugs to provide selectivity.
Some other benefits can be deduced from Figure 1.10, where the total mass attenuation coefficient of gold and water are plotted, assuming human tissues as soft tissue.

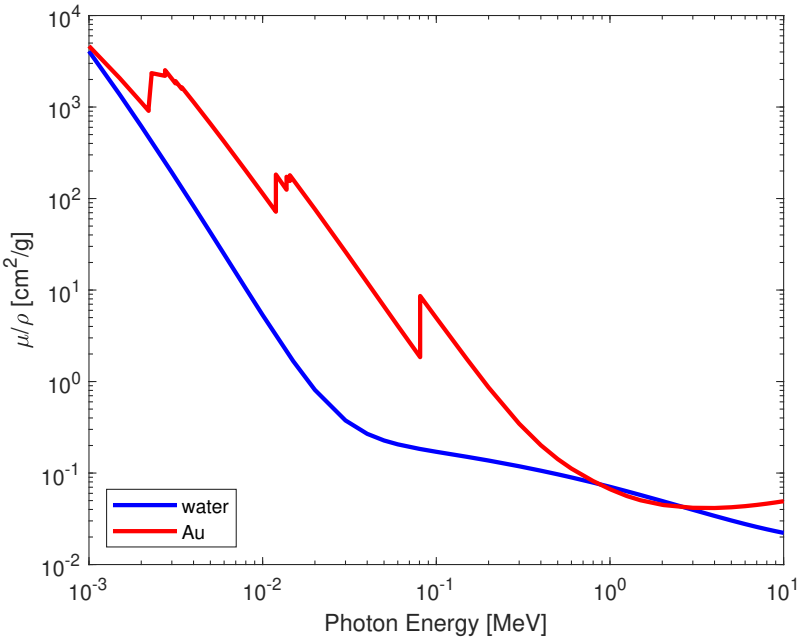

Figure 1.10: Total mass attenuation coefficients for gold and water, with values taken from the NIST XCOM database. The human tissues are made by 70% of water, so water represents a good approximation as soft tissue.[47]

For higher-energies, between 1 and 10 MeV, and very low doses the differences between the two curves is irrelevant meaning there are no advantages in the dose enhancement. While for intermediate energies between 2e-3 and 1 MeV, secondary electrons coming from the de-excitation of the Au can lead to fluorescence and Auger electrons enhancing the dose delivered. These electrons may be confined within the cell, preventing the exposure of the surrounding healthy tissues and so achieving the purpose to prevent healthy cell from radiation damages. However, Auger electrons may deliver a relatively high local dose, while fluorescent photons can have enough energy to travel further in the tissue, causing a dose delocalization in the surrounding cellular environment.[25]

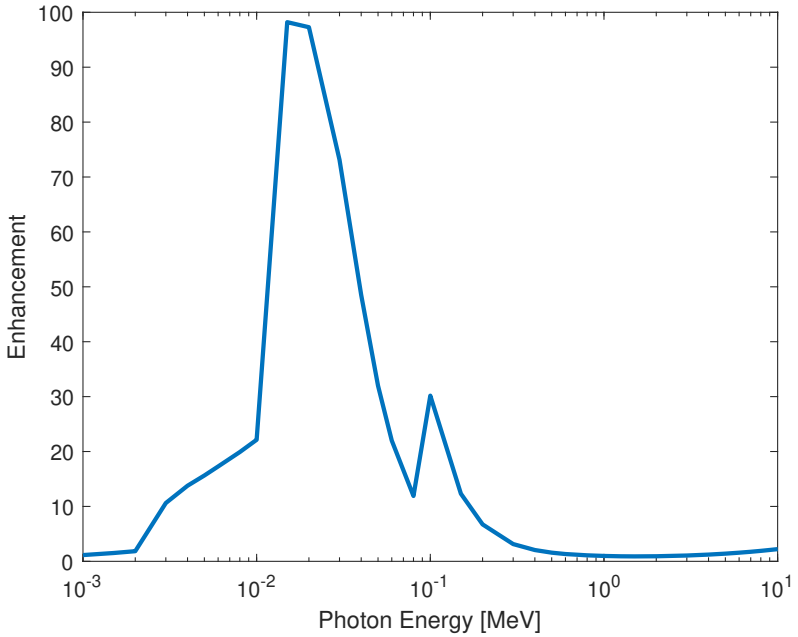

Figure 1.11: Enhancement of energy absorbed from the fraction between the total mass attenuation coefficients of gold and water, with values taken from the NIST XCOM database.[47]

Figure 1.11 shows clearly the enhancement of photon interactions for different energy beam, i.e., gold absorbs higher energy than soft tissue that results in an enhancement in the local dose when a small dose is delivered to gold. An ideal radiosensitizer should be able to upgrade the IR effects in the tumor region, minimizing the level of intrinsic toxicity. In this regard, AuNPs show a low toxicity and also a high chemical stability and compatibility. The IR upgrades is correlated to the particle dimensions and concentration. Generally, the ROS production increases for small dimensions because of an higher surface area to volume ratio that leads to an higher electron emission.[28] [32] [51] Finally, AuNPs can inhibit the DNA repair under irradiation , usually stronger in cancer cells that in healthy cell, mediating the bystander signalling. Gold absorbs higher energy than water/soft tissue, which can increase the localised dose delivered to tumor.[22]

1.7 Brain Tumor

Central Nervous system (CNS) tumors are one of the most recurrent tumor diseases in the world. There are many different types of CNS tumors, some are cancerous and often very aggressive or high grade. Brain tumors are the biggest cancer cause of death among children and adults under 40. Based on data available, the global incidence of malignant brain tumors is 4.25 cases per 100.000 person-years, which vary by region from 6.76 in Europe to 2.81 in Africa.[24] Due to its location, this kind of tumors can lead to the damage and/or the disruption of the entire body functioning, hence the conventional treatment modalities are not efficient.[26] glioblastoma, a high grade brain tumor occurring in the frontal and temporal lobe, also called glioblastoma multiforme (GBM), belongs to this category. (Figure 1.12) GBM represents the 15% of all primary brain tumors of grade IV and is predominantly made up of abnormal astrocytic cells, although also contains a mix of different cell types (including blood vessels) and areas of dead cells (necrosis).

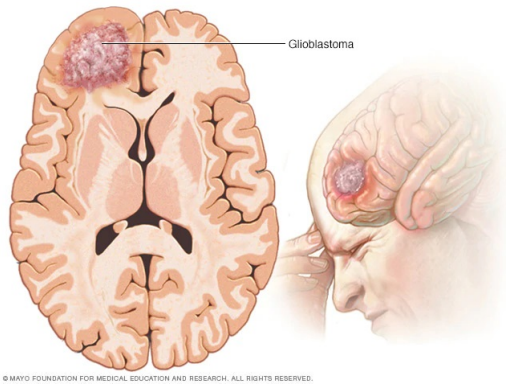

Figure 1.12: Gliobastoma location in central tumor system. [55]

It is characterised by an overexpression of the neurokinin-1 (NK-1) receptor. [3][11]The WHO distinguishes GBM as primary , a distinct entity, or secondary Glioblastoma, a progression form of a previous astrocytoma. Both types of GBM show loss of genetic material on chromosome 10 and the amplification of the Epidermal Growth Factor Receptor (EGFR) which make GBM very invasive and able to proliferate into nearby areas or spread to the opposite side thanks to connection fibres. Radiation therapy, in this case, is able to slow down the growth of GBM that cannot be completely removed by surgery.[3][13][16] Glioblastoma is an intrinsically radioresistant cancer and for this reason the treatment is often palliative.[12][33] In order to reduce the radioresistance of the GBM and enhance the effect of the radiotherapy, the use of gold as radiosensitizers have been studied and reported in several works.

Bobyk et al. (2013) studied the efficacy of AuNPs as radiosensitizers for low energy beams (88 keV). The F98 glioma (rat glioma) cells were tested with NPs of 1.9 and 15 nm diameter. The cells, with a concentration of 10 mg Au/mL were irradiated with a total dose of 6 Gy (dose rate of 0.5 Gy/s). They obtained a dose enhancement factor (DEF) of 1.92 and 1.40 for 1.9 and 15 nm diameter NPs respectively.[27]

Joh et al. (2013) studied the use of AuNPs of 1.9 nm diameter in the human brain tumour U251 cells. The U251 cells, incubated with a concentration of 1 mM AuNPs were irradiated using a 150 kVp source for a total dose of 4 Gy, being estimated a DEF value of 1.3.[15]

Taggart et al. (2014) studied AuNP-mediated radiosensitizers of 1.9 nm diameter at a concentration of 0.5 mg/mL in different cell lines, including the human brain tumor cells T98G. The cells were irradiated with 225 kVp χ-rays showing a DEF decrease with an increase of the total absorbed dose. The dose was increased between 2 and 8 Gy resulting in a DEF in the range 1.90-1.35.[29]

Kazmi et al. (2020) evaluated the radiosensitization effect of AuNPs of 42 nm diameter effect in U87 GBM cell lines, upon irradiation with a 6 MeV photon beam. A concentration of 100 µg/mL showed a DEF of 1.45 for 2 Gy dose.[18]

Finally, Mendes et al. (2020) synthesised and studied AuNPs,with a core size of 4-5 nm diameter, combined with the peptides SP and TyrSP (SP =Substance P) as target specific nanoparticles, taking advantage of the SP affinity for the NK-1 receptor that allows a better internalization of the AuNPs in GBM cells. The study evaluated the potential of the SP-functionalized AuNPs for image-guided chemo-radiotherapy of Glioblastoma in different cell lines. In particular, these gold nanoparticles when labeled with ^{67}Ga (^{67}Ga-AuNP-SP) showed a high internalization rate in the GBM cell line T98G: about 30% of internalization in the first ten/fifteen minutes of incubation. It was observed a surface bound fraction about only 5% , with a total cellular uptake of 37%.[45](Figure 1.13) .

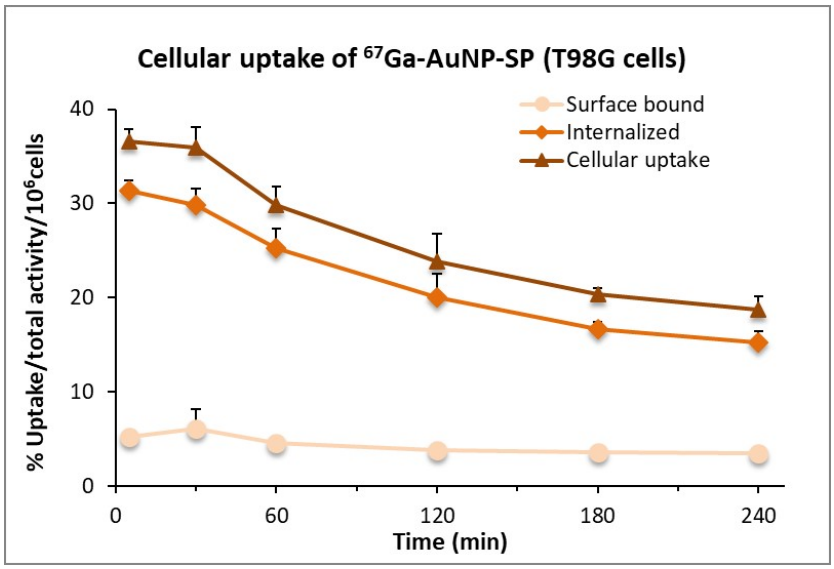

Figure 1.13: Cellular uptake of ^{67}Ga-AuNP-SP in the T98G cell line. Data obtained from experimental studies done at C^{2}TN/IST [45]

1.8 Aim of the work

The properties of gold nanoparticles make them useful for theranostics purposes combining therapeutic and diagnostic functions, as summarized below [22][25][28][32][37]:

- Low toxicity;
- Good biological compatibility;
- Easy synthesis with a wide range of sizes;
- Effective dose enhancement due to the high atomic number;
- Good internalization in tumor cells;
- Possibility to be labeled with imaging agents;

Initially, the aim of the thesis was to evaluate the potential of AuNP-TDOTA-SP as radiosensitizers for the treatment of glioblastoma based on experimental and computational approaches. The AuNPs cited are the same mentioned by Mendes et al. (2020) and were synthesised at C^{2}TN following the procedure shown in Figure 1.14 .

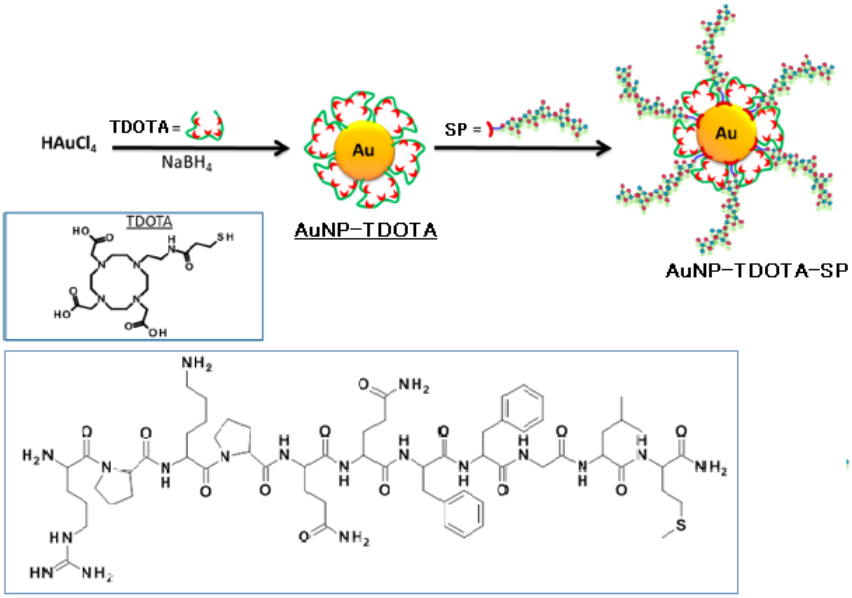

Figure 1.14: Synthesis of AuNP stabilized with TDOTA and the SP peptide. Adapted from Silva et al. (2016).[20].

However, due to the limitations imposed by the Covid-19 crisis, the thesis is focused only on computational studies. The role of computational studies on radiobiological and dosimetric effects of radiosensitizers is mainly focused-in understanding in what extent the presence of nanoparticles inside tumor cells can cause a dose enhancement (that can results in a greater efficiency for cancer cells killing). Specifically, given the experimental complexity related to the measurement of dose enhancement effects due to the not homogeneous distribution of AuNPs in cells and tissues, computational tools permit to estimate the increase of dose delivered to cell using several radiosensitizing materials (such as AuNPs).[17]

Simulations can be set considering different parameters (such as cell geometry, source beam, type of particle and material) in order to reproduce the irradiation set up of experimental studies and to understand which could be the best configuration that would permit an higher dose enhancement effect. With the use of AuNPs, the DEF occurs close to the nanoparticles thanks to the contribution of ejected photoelectrons and de-excitation process leading to a local electronic perturbation.[56] In this way, the use of AuNPs, depending on the particle location, can be very effective also in minimizing the dose to the surrounding healthy tissues, where the administration of dose should be avoided.[56] Taking advantage from simulations is possible to numerically predict this DEF and see in which volume occurs, for what concentration of AuNPs, and if it occurs preferentially in the AuNP or in the surrounding volumes, corresponding to the cell culture media. The aim of the thesis is to predict how gold nanoparticles influence the dose distribution inside glioblastoma cells by calculating the dose enhancement factor in different possible configurations and using a $_{60}$Co photon and a 50 kV χ-ray source. This computational optimization study, in prospective , will be usefull for complementary experimental works with AuNPs irradiated by ^{60}Co. Towards this goal, the state-of-the art PENELOPE/PenEasy package Monte Carlo code was used for calculations where parameters, such as photon energy, cell size and intracellular localisation were tested, taking also into account the experimental results about cellular uptake (with the AuNPs type that were thought to be used in this thesis work) obtained by Mendes et al. (2020).

Chapter 2

Material and methods

In this chapter the material and methods used for the development of the Montecarlo simulations are briefly described. Each analysis performed is motivated and described taking advantage of table and images that leads to a better understanding of the assumptions and processes adopted.

2.1 Monte Carlo methods

The Monte Carlo methods represent a wide class of computational algorithm that adopt repeated random sampling to obtain numerical results. The first use of a Monte Carlo method dates back to the second world war in Los Alamos where research scientists was working on mathematical physics and the atomic bomb. [7] Monte Carlo techniques can be applied to radiation transports, statistical, physics and many-body quantum theory. These methods can be applied to simulate the behavior of some particles, like electrons, ions, photons and so on, in the human body in order to understand what are their interactions and the consequent effects. This behavior is described by the Boltzmann Linear Transport equation that MC methods are able to solve following accurately each particle through complex geometry.[57] The technique consists in a generation of random numbers applied to a probability function describing the particle probability to have a certain interaction in the medium, during which changes of directions, loss of energy and secondary particles can be produced. The history of the particle, also called track, is a random free flights sequence ending with an interaction having an associated probability function.[19] Generally simulations of realistic number of particle histories is not feasible due to fine computational speed and memory, for this reason variance reduction techniques are usually used to decrease the number of histories required for a low statistical uncertainty.[57] The most used MC package used for radiation-physic purpose are PENELOPE, GEANT4, FLUKA, MCNP. [10] In this work the PENELOPE code package was implemented for MC simulations.

2.2 FORTRAN Programming Language

FORTRAN is a programming language used for scientific and engineering computing applications. It was first used to convert mathematical notation to machine instruction in 1954 at the International Business Machines Corporation. The name FORTRAN is an acronym of

"formula translation" enclosing the program functionalities and the reason of its large implementation in many computers after its first use. During the years, the program has been updated many times so that FORTRAN exists in several version such as FORTRAN66, FORTRAN77, FORTRAN90, FORTRAN95 and FORTRAN2003. However FORTRAN remains the principal language for scientific and engineering computing applications. FORTRAN programming language is used to write the PENELOPE/PenEasy package. [23]

2.3 PENELOPE

PENELOPE is an abbreviation of PEnetration and Energy Loss of Position and Electron. It is an open source, free package that allows to make MC simulations of radiation transport of photons, electrons and positron in complex geometries and materials in the energy range 50 eV to 1 GeV. The transport processes and so large part of PENELOPE are built using a set of FORTRAN95 subroutines. This means that a main program must be provided by the user to work. The PENELOPE code package consists in six subroutines:

- penelope.f: to simulate radiation transport in homogeneous material;
- pangeom.f: to track particles within modular quadratic geometry;
- penvared.f: to apply basic variance-reduction methods;
- rita.f: to sample random numbers;
- material.f: to create material files;
- timer.f: to measure simulation time.[19]

2.4 PenEasy

PenEasy is the main program used in this work for PENELOPE package. It is also free, open source and written in FORTRAN95. Some PenEasy packages contained are:

- penEasy.F: containing the source code;
- penaux.F: containing subroutines to help penEasy run;
- penvr.F: cont
- tally*.F: containing subroutines to implement each PenEasy tally.

The version used is the 2019-09-21 operating with PENELOPE 2018 version. PenEasy package is chosen because of its specific tallies, in particular the energy deposition tally get out the energy deposition for each material and the spherical dose distribution gives the dose deposited in each spatial bins.[53][4] The operation of the package is based on an input file an output file. The input file allows to set quantities relative to the simulations and call files as the geometry one. It is divided in several sections:

- *SECTION CONFIG.*: set general parameters of the simulation like number of histories and the available time;

- *SECTION SOURCE BOX ISOTROPIC GAUSS SPECTRUM*: set the source parameters , defined the type of particles (electrons (1), photons (2) or positron (3)), the box center coordinates and the box sides in x, y and z, the direction and the beam shape and the energy spectrum;
- *SECTION PANGEOM + PENVOX*: to call the geometry expressed in a *.geo file if it is quadratic or *.vox if it is voxelized. In these files the information about the material are also specified;
- *SECTION PENELOPE*: to define material file created using material.f. Each line is defined by the material expressed in *.mat and several parameters determine the accuracy and simulation speed. (Table 2.1)
- *TALLY SECTION*: set on or off various tally section;
- *SECTION INTERACTION FORCING*: set the forcing of a certain interaction (ICOL) in a material (MAT) for a certain kind of particles (KPAR).

Table 2.1: Parameters set in SECTION PENELOPE of PenEasy.

Parameter	Meaning
EABS(e-), EABS(ph), EABS(e+)	Cut energy for electrons, photons and positrons. The particle is considered absorbed when it reaches this value so no more history track is generated.
C1 , C2	Average angular deflection produced and maximum average fractional energy loss between two consecutive elastic event
WCC, WCR	cutoff energy for inelastic collision and bremmstrahlung emission (eV)
DMSAX	maximum allowed flight length for electrons and positrons.

The PenEasy output file gives a report of the simulation, giving information about how the input PenEasy file is read and about the simulation itself like simulated number of particles and simulation speed. The results of each tally adopted are reported in separate files, e.g. expressed in *.dat extension. The tallies used in this work are[53][19]:

- Energy Deposition Tally: reporting energy deposited in each material defined in SECTION PENELOPE, along with uncertainty and the two standard deviations. The results are expressed in (eV/history);
- Spherical Dose Distribution Tally: reporting the Dose deposited (eV/g/history) in each spatial bins, which volume is defined by the user, the low and the average radius (cm) and the two standard deviations.

2.5 Secondary particles equilibrium

The secondary particle equilibrium is one of the fundamental issues to consider in Monte Carlo simulations for local enhancement study in presence of gold nanoparticles. If this condition is not considered or not reached at all, the results may be biased and overestimated. Simulation of beam geometries limited to the dimension of nanoparticles are far from the reality where the beam size is of the order of millimeters, however real beam sizes are not computationally feasible. In this regard there is a lateral lack of secondary particles equilibrium that must be taken into account to consider how interpret the results.[21]
There are three effects lost when the beam width is unreal and smaller than the range of secondary electrons:

- The contribution of electrons generated by photon interactions outside the confined beam simulated is not considered. In the reality these electrons can deposit energy in the volume used for scoring, consequently there will be an underestimation of the real absorbed dose.
- The Compton and Rayleigh scattered photon interactions with the AuNPs is underestimated. With this contribution a net increase of the Dose Energy Fraction is expected;
- AuNPs can lead to the absorption of electrons produced outside the irradiated beam area. This effect should reduce the DEF but considering the first two effects can be considered irrelevant.[21]

2.6 Validation of the model

The validation process is done to check if the model is correctly implemented with respect to the literature results in irradiation studies. In particular the study "Intercomparison of dose enhancement ratio and secondary electron spectra for gold nanoparticles irradiated by 50kVp χ-rays calculated using multiple Monte Carlo simulation codes" done by Li et al. (2020) [35] and "Irradiation of gold nanoparticles by χ-rays: Monte Carlo simulation of dose enhancements and the spatial properties of the secondary electrons production" done by Leung et al.(2011)[30] are used as reference models according to the simulation parameters set. For the calculations, the parameters below are chosen and fixed considering their relevance at nano-scale and micro-scale:

- Interaction forcing for gold nanoparticle set to 1.5 in order to consider the production of low energy electrons from photoelectric and Auger effect;
- DSMAX set to 1/10 of the material thickness;
- cut-off energy set to 50 eV for all particles.

2.6.1 Energy deposition validation

The first validation is made considered the fraction of energy deposited externally to the AuNPs for different size of gold nanoparticle. Adapting the Leung et al. (2011) method the simulations were setting considering a single gold sphere nanoparticle centered in a water tracking volume irradiated by the ^{60}Co photon source parallel to the y-axis emitting rays parallel to the z-axis. Figure 2.1 shows the irradiation configuration while the set of parameter used are reported in Table 2.2.[30]

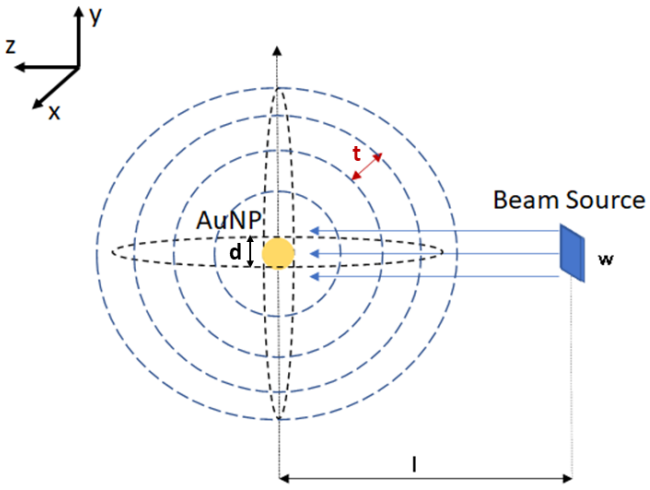

Figure 2.1: Geometry setup for the energy deposition model validation. A single AuNP is centered in liquid water shells. Parallel rays, produced by a ^{60}Co source, are sampled from a planar square area with a length w equal to the AuNP diameter. The AuNP is irradiate along the z-axis in a right-handed Cartesian reference frame at a distance l between the center of planar square source and the center of the AuNP. The dose is scored in concentric spherical shells of thickness d around the AuNP.

Table 2.2: Setting geometry specifications for the Energy deposition validation.

	Geometry	Dimension	Location
AuNP	Sphere	Diameter (d) 2, 50, 100 nm	centered in the axes origin
Source beam ^{60}Co	Planar square rays parallel to z-axis	Width (w) 2, 50, 100 nm	Distance (l) 1 mm
Water track volume	Cubic	Side 22 mm	centered in the axes origin
Water detecting volumes	shells # 150	Thickness (t) 40 µm	Concentric to AuNP

The side of cubic tracking volume was chosen equal to 22 mm considering that ^{60}Co is one of the most energetic sources present in the Leung et al. (2011) model. The Energy Deposition Tally was used to extract the energy in the AuNPs, whereas for the shells the absorbed dose was first detected in 150 homogeneous steps from the external AuNP radius up to 0.6 cm using the Spherical Dose Distribution Tally. Then, using mathematical calculations, the energy in the first 5 shells is extracted. For this analysis, the simulations were stopped when reached 2.5×10^7 number of histories, i.e. the number of primary particles generated.

2.6.2 DEF assessment method

The Dose Enhancement factor for the irradiated cells is calculated for each shell as the fraction between the deposited Energy in each shell (in eV/hists unit) with the gold nanoparticles (E_{Au}) and the deposited Energy in each shell with the volume occupied by AuNPs filled by water (E_{H_2O}, considering the relationship between Dose and Energy. (Equation 1.1)

$$DEF = \frac{E_{Au}}{E_{H2O}} \quad [-] \tag{2.1}$$

The programs give as output a *.dat file containing the energy in each material and its uncertainty express as 2 times the standard deviation (δE). The absolute uncertainty of the Energy (δE) is obtained dividing the value of the uncertainty (δE) in the material by the value of the respective energy (E):

$$\delta E\% = \frac{\delta E}{E} \times 100 \tag{2.2}$$

While the absolute uncertainty on the DEF (δDEF) is obtained with the following equation:

$$\delta DEF = \sqrt{(\frac{1}{D_{H2O}})^2(\delta D_{AU})^2 + (\frac{1}{D_{H2O}})^4(\delta D_{H2O} D_{Au})^2} \tag{2.3}$$

$$\delta DEF\% = \frac{\delta DEF}{DEF} \times 100 \tag{2.4}$$

2.6.3 DEF validation

This procedure is done in order to validate the Dose Enhancement Factor with different kind of sources. Adapting the Li et al. (2020) method the simulations were set by irradiating a single gold nanoparticle centred in a liquid water shell, irradiated by the source parallel to the y-axis emitting rays parallel to the z-axis. The irradiation scheme is shown in Figure 2.2 while the parameter specifications are described in the Table 2.3. [35]

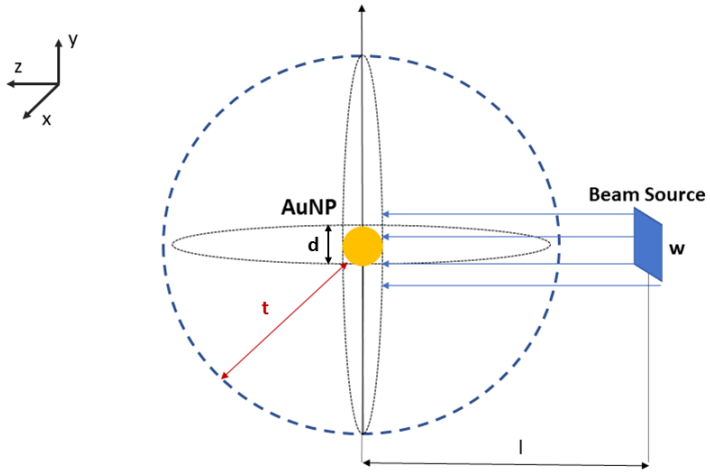

Figure 2.2: Geometry setup for the DEF model validation. A single AuNP is centered in liquid water shells. Parallel rays, produced by an χ-ray or ^{60}Co source, are sampled from a planar square area with a length w. The AuNP is irradiate along the z-axis in a right-handed Cartesian reference frame at a distance l between the center of planar square source and the center of the AuNP. The energy deposition is scored in a concentric shells of thickness t around the AuNP.

Table 2.3: Setting geometry specifications for the DEF validation.

	Geometry	Dimension	Location
AuNP	Sphere	Diameter(d) 100 nm	centered in the axes origin
Source beam ^{60}Co/50 kVp χ-ray	Planar square rays parallel to z-axis	Width (w) 110 nm	Distance (l) 1e-4, 1e-2, 1e-1, 1 cm
Water track volume	Cubic	Side 4 mm	centered in the axes origin
Detecting water volume	Shells	Thickness (t) 1 µm	concentric to AuNP

In addition to the Li et al. model (2011), the AuNP-source distance (l) was varying to understand how the longitudinal secondary electron equilibrium effects the DEF results,

stopping the simulations when the number of histories was reached the value of 1×10^7.

The Energy Deposition Tally was used to extract the energy in the micrometer water shell with and without gold useful to calculate the respective DEF.

2.7 Simulation set up for DEF calculations

Taking advantage of the validation simulations, the study of the Dose Enhancement factor for different cell size and concentration was set considering:

- AuNPs cellular internalization equal to the 30%;
- 50 kVp χ-ray and ^{60}Co sources;

The two energy sources were chosen in order to see the trend of the Dose Enhancement Factor changes taking into account that for gold the photoelectric effect is maximized in 50 - 200 keV. As for the validation of the model the following parameters are chosen and fixed considering their relevance at nano-scale and micro-scale:

- Interaction forcing for gold nanoparticle set to 1.5 in order to consider the production of low energy electrons from photoelectric and Auger effect;
- DSMAX set to 1/10 of the material thickness;
- cut-off energy set to 50 eV for all particles.

2.7.1 Sensitivity study of beam width effect on DEF

Since the prohibitive computational time required to obtain DEF results with wider beam (see section 2.5), a sensitive study was performed in order to understand the overestimation extent when using narrow beams. In this way, even when obtaining results with narrow beam, it is possible to understand more closely the order of magnitude of real DEF. It is safe to remark also that these results take into account only the physics of the dose enhancement effect (radiation-matter interaction), whereas for a complete DEF assessment some radiobiological studies should be performed.[21] The irradiation scheme used for this analysis is reported in Figure 2.3 while the set parameters are reported in Table 2.4.

Table 2.4: Setting geometry specifications for the DEF validation.

	Geometry	Dimension	Location
AuNP	Sphere	Diameter(d) 100 nm	centered in the axes origin
Source beam 50 kVp χ-ray ^{60}Co	Planar square rays parallel to z-axis	Width (w) 100 µm, 1 µm, 150 nm 1 µm, 150 nm	Distance (l) 100 µm from AuNP 100 µm, 1 cm from AuNP
Water track volume	Cubic	Side 4 mm	centered in the axes origin
Detecting water volume	Shells #15	Thickness (t) 100 nm	concentric to AuNP

For this part the geometrical assessment was done implementing the two configurations used for the Validation of the model with some improvements, in particular:

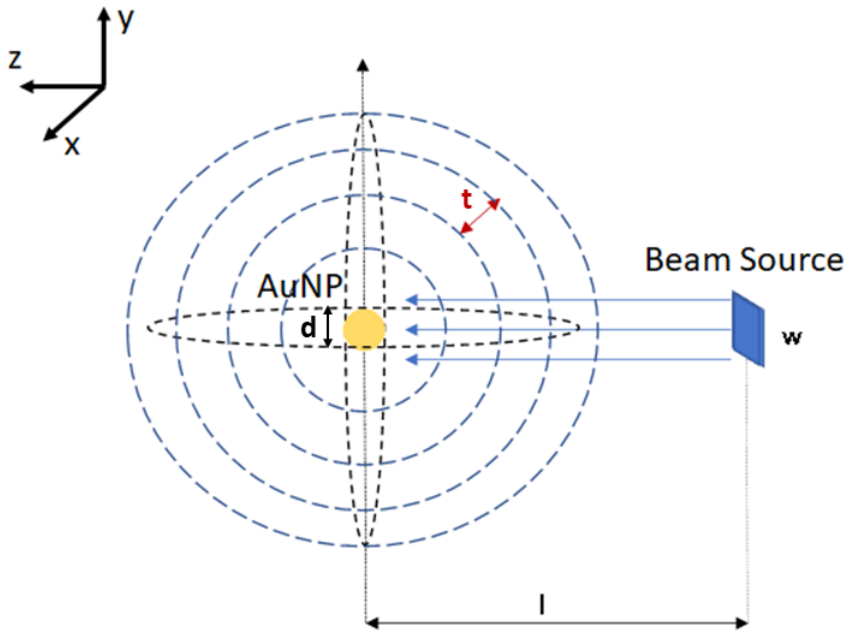

Figure 2.3: Geometry setup in for sensitivity study. A single AuNP with a diameter of 100 nm is centered in liquid water. Parallel rays, produced by a χ-ray or ^{60}Co source, are sampled from a planar square area with a length w of 100 µm or 1 µm. The AuNP is irradiate along the z-axis in a right-handed Cartesian reference frame. The distance l between the center of planar square source and the center of the AuNP is 100 µm. The energy deposition is scored in concentric spherical shells of thickness d around the AuNP.

- the beam width was always larger than the AuNP diameter in order to reduce the longitudinal secondary particles non equilibrium;
- the cubic world size was reduced to 4 mm for both sources considering the source located still inside the world: from some initial attempts the world seems not effect the results providing the source is located inside it;
- the shell thickness was reduced to 100 nm considering the interest of treatment planning on nanometer to micrometer dose enhancement;
- the simulations were stopped when the number of histories reached the value 10^8-10^9 considering the few photons interactions in the tissue for clinically relevant energy (mean free path up to 40 g cm^{-1}).[57]

Moreover, the differences in ^{60}Co and 50 kVp χ-ray sources, makes the simulation of the 100 µm width source unfeasible for the ^{60}Co due to the high computational time and the correlated high uncertainties, for this reason only the beam widths of 1 µm and 150 nm are used for the ^{60}Co rays. In addition, one more simulation for ^{60}Co is performed respect to 50 kVp χ-ray source, considering a AuNP-source distance of 1 cm that should assure the longitudinal electron equilibrium.[57] The average DEF in the 15 shells is obtained using the 'mean' Matlab function for 1 cm and 100 µm source distance.

2.7.2 Concentration study: Number of particles calculation

In order to model gold nanoparticles characteristics consistent with the real AuNPs used at C^2TN/IST, the data obtain by a TEM acquisition done on the AuNPs-TDOTA were considered for an estimate of the nucleus diameter dimension. The acquired image and the respective histogram are showed in Figure 2.4.

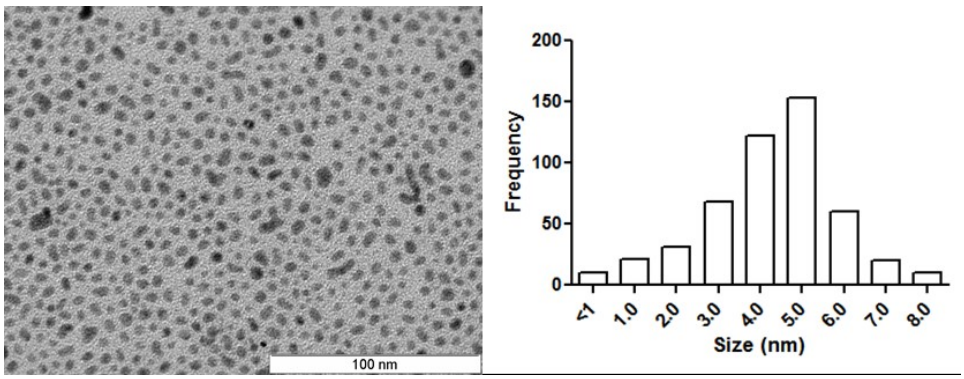

Figure 2.4: TEM images for AuNPs-TDOTA and respective histogram.

According to these data, the AuNP-TDOTA has an average diameter size of 4.29 nm. In order to estimate the number of AuNPs a concentration of 37.5µg/mL was considered and so 7.5µg/200 µL, taking into account the volume of a 96-well plate well to use for the real irradiation. The number of spherical AuNPs per cell is calculated considering the following data:

- % internalization/10^6 cells after 30 minutes: 30%;
- Gold density: 19.32 g/cm^3;
- Au mass in AuNP-TDOTA: 30.6% of the whole mass;
- AuNP-TDOTA concentration: 37.5µg/mL.

The following calculations are made to achieve the number of AuNP/cell:

$$\%Internalization/8000cells = \frac{\%Internalization/10^6 * 8000}{10^6} \tag{2.5}$$

$$CAI = \%Internalization/8000cells * 0.01 * 7.5 \quad [\frac{\mu g}{200\mu L}] \tag{2.6}$$

$$V_{Au} = \frac{4}{3}\pi R^3 \quad [cm^3] \tag{2.7}$$

$$M_{Au} = V_{Au}\rho \quad [g] \tag{2.8}$$

$$M_{NPs} = \frac{M_{Au}}{0.306}[g] \tag{2.9}$$

$$CAI_n = \frac{CAI * 10^-6}{M_{NPs} * 8000} \quad [\frac{AUNPs}{cell}] \tag{2.10}$$

$$\frac{NPs}{mg} = 0.001 M_{NPs} \tag{2.11}$$

$$\frac{Au}{mg} = 0.001 M_{Au} \tag{2.12}$$

$$M_{cell} = \rho_w Vol_{cell} \quad [mg] \tag{2.13}$$

$$AuNPs = M_{cell} \frac{Au}{mg} \tag{2.14}$$

Where:

- CAI is the concentration after the internalization with the mass of nanoparticles;
- V_{Au} is the volume of the gold nanoparticle;
- M_{Au} is the mass of the gold nanoparticle;
- M_{NPs} is the mass of the whole nanoparticle;
- CAI_n is the concentration after internalization with the number of nanoparticles;
- M_{cell} is the mass of the different cell;
- ρ_w is the water density;
- Vol_{cell} is the volume of the cell;
- AuNPs is the number of nanoparticles for each cell volume considering only the gold sphere.

Table 2.5 reports the number of nanoparticles obtained for each cell dimensions considering a constant internalization of 30%. The calculations are done considering only the gold core of the nanoparticles that is the one useful for the simulations purposes.

Table 2.5: Number of gold nanoparticles for each cell size, 37.5 µg/mL

Cell diameter [µm]	AuNPs
10	6.54×10^5
15	2.21×10^6
25	1.02×10^7
50	8.18×10^7

2.7.3 Geometries and Source Definitions

Due to the high number of AuNPs obtained from calculations it was chosen to simplify the simulating model by considering a single AuNP or a gold shell. In this case, the diameter and thickness dimensions of the single AuNP/shell are chosen by considering the equivalence between the volume of the cluster of AuNPs estimated through TEM and the single AuNP/shell. The dimension of the cells containing the gold nanoparticles are chosen according to other reports in the literature. [31][41] Due to the different possible dimension and morphology of tumor cells, two concentric spheres, one for the nucleus and one for the cytoplasm, are simulated, considering the nucleus volume equal to the 8% of the cell volume.[41] The nucleus and cytoplasm diameter for each cell are reported in Table 2.6.

Table 2.6: Specification of cells size: cytoplasm and nucleus diameter calculated taking advantage of Huber (2007) work.[41]

Cell diameter [µm]	Nucleus diameter [µm]
10	4.31
15	6.46
25	10.77
50	21.54

The dimensions of a single AuNP or the gold shell are obtained considering a constant AuNPs internalization of 30% (see 1.13) and the following distribution nucleus-cytoplasm:

- 100% - 0%;
- 0% - 100%;

The value of internalization is chosen considering that the experimental part was supposed to test the effects on T98G cells irradiated for 6/7 minutes to achieve a total dose of 5/6 Gy. The source beam is defined as in the sensitivity study part, i.e. a square plane parallel to the y-axis emitting rays parallel to the z-axis at a distance of 100 µm for 50 kVp χ-ray source and 1 cm for the ^{60}Co source. (Figure 2.3) Taking advantage of the sensitivity study, the source width was set 20 nm higher than the AuNP/gold shell diameter, while the shells used to detect the energy deposition were set with a thickness of 100 nm but have different number and location considering the different nucleus-cytoplasm concentration configuration.

Table 2.7: Number of AuNPs for each cell size with the equivalent AuNP and gold shell dimensions used in the concentration study.

Cell diameter [µm]	AuNPs	AuNP equivalent diameter [nm]	gold shell equivalent thickness [nm]
10	6.54×10^5	372	0.463
15	2.21×10^6	559	0.696
25	1.02×10^7	930	1.16
50	8.18×10^7	1862	18.5

Configuration 100%-0% nucleus-cytoplasm

For this concentration configuration study a single gold nanoparticle located in the center of the cell nucleus was considered. The diameter length is calculated using the Excell function "objective search" imposing the condition that the fraction between the volume of the big AuNP and the volume of the small AuNPs with a diameter of about 4.29 nm is equal to the number of AuNPs corresponding to the 30% of internalization for each cell. (Table 2.8) The Energy Deposition Tally is used to detect the energy in 30 shells in the nucleus of 100 nm thickness guaranteeing a DEF map in the first 3 µm from the AuNP. (Figure 2.5)

Table 2.8: AuNP geometry and source beam specifications for the concentration nucleus-cytoplasm 100%-0% in the different cells dimension considered.

Cell diameter [µm]	AuNP diameter [nm]	Beam width [nm]
10	372	400
15	559	580
25	930	950
50	1862	1882

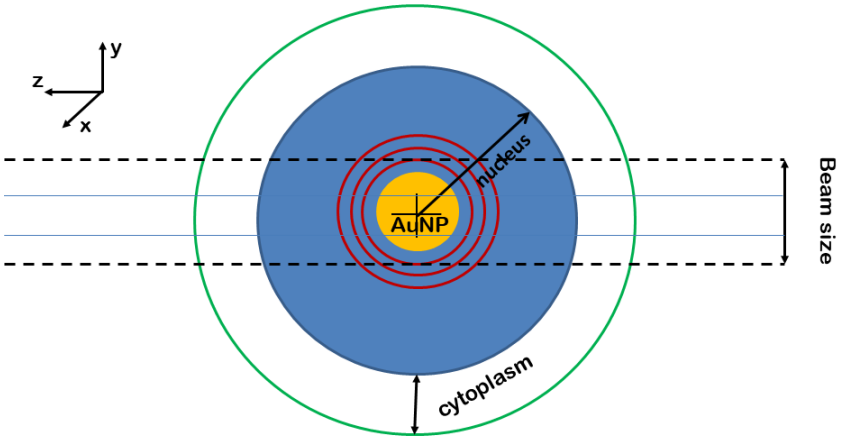

Figure 2.5: Geometry setup for MC simulation: 30% constant internalization with nucleus-cytoplasm configuration 100%-0%. A single AuNP corresponding to a cluster of AuNPs (with diameter of 4.29 nm each) is centered in liquid water corresponding to the nucleus. Parallel rays, produced by a 50 kVp χ-ray or ^{60}Co source, are sampled from a planar square area with a width 20 nm higher than the AuNP. The AuNP is irradiated along the z-axis in a right-handed Cartesian reference frame. The energy deposition is scored in concentric spherical shells of thickness 100 nm around the AuNP.

Configuration 0%-100% nucleus-cytoplasm

For the configuration with the 100% of AuNP located in the cytoplasm a gold shell located in the cytoplasm with the small diameter equal to the nucleus membrane was considered. Its thickness and the external diameter is calculated using the Excell function "objective search" imposing the condition that the fraction between the volume of the gold shells and the volume of the small AuNPs with a diameter of about 4.29 nm is equal to the number of AuNPs corresponding to the 30% of internalization for each cell. (Table 2.9) The Energy Deposition Tally is used to detect the energy in 20 shells in the nucleus and 20 shells in the cytoplasm of 100 nm thickness guaranteeing a DEF map in the 2 µm far from the gold shell in the nucleus and in the cytoplasm. (Figure 2.6)

Table 2.9: Geometry gold shell and source beam specifications for the concentration nucleus-cytoplasm 0%-100% in the different cells dimension considered.

Cell diameter [µm]	Nucleus diameter [µm]	Gold shell thickness [nm]	Beam width [µm]
10	4.31	0.463	4.33
15	6.46	0.696	6.48
25	10.77	1.16	10.8
50	21.54	18.5	21.6

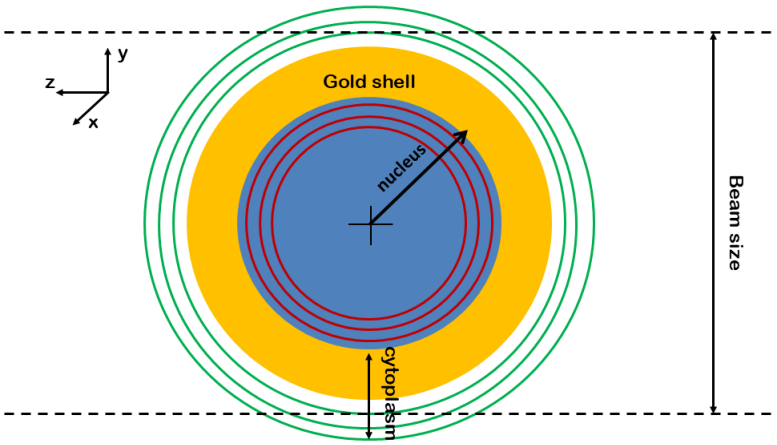

Figure 2.6: Geometry setup for MC simulation: 30% constant internalization with nucleus-cytoplasm configuration 0%-100%. A gold shell corresponding to a cluster of several AuNPs (of 4.29 nm diameter each) is located close to the nuclear membrane. Parallel rays, produced by a 50 kVp χ-ray or ^{60}Co source, are sampled from a planar square area with a width 20 nm higher than the AuNP.The AuNP is irradiate along the z-axis in a right-handed Cartesian reference frame. The energy deposition is scored in concentric spherical shells of thickness 100 nm around the gold shell in the nucleus and in the cytoplasm.

2.7.4 Materials Definition

The material files used to run the MC simulations are obtained from the PENELOPE package material database, through the material.f program. The Table 2.10 reports the type of materials listed in the PENELOPE section of the input file.

Table 2.10: Material list present in the PENELOPE section of the PenEasy input file.

Material	Density [g/cm^3]	Geometry component
water	9.9821×10^{-1}	cell shells and outer cube
gold	0.01932×10^{-1}	AuNPs and gold shells

The energy in each material defined in the PENELOPE section of the input file. Even if the shells are made all by the same material, a different material file needs to be created for each geometry component in which the energy is deposited to prevent misinterpretation. Figure 2.7 shows the geometry build in the *.geo file used for the simulations with the numbered material corresponding to each geometry.

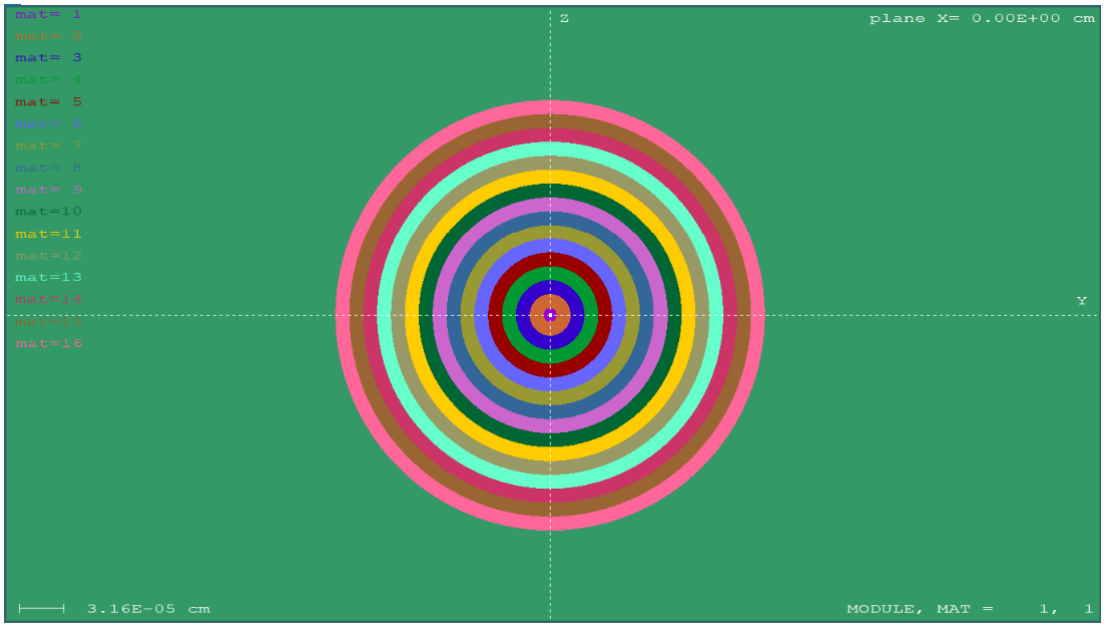

Figure 2.7: Representation of a cross section of the cell passing through the x=0 plane, using the quadratic geometry viewing program gview2d. The outer cube is represented with the outside green.

2.8 Spectrum Definition

The two spectra used to simulate the irradiation are briefly described. The same spectra are used both for the validation process and the simulation itself.

2.8.1 ^{60}Co source

The ^{60}Co is a radioactive isotope with an half-life of 5.26 years. It decays through β^- emission with an energy of 0.31 MeV for an excited ^{60}Ni and with energy of 1.173 MeV and 1.332 MeV for a stable state. The 99.88% of β^- decay from ^{60}Co to the second excited state ^{60}Ni with a maximum electron energy of 0.313 MeV, while the 0.1% decay from ^{60}Co to the first excited state ^{60}Ni with a maximum energy of 1.486 MeV. The ^{60}Co is artificially produced by neutron radiative capture reaction.[48]

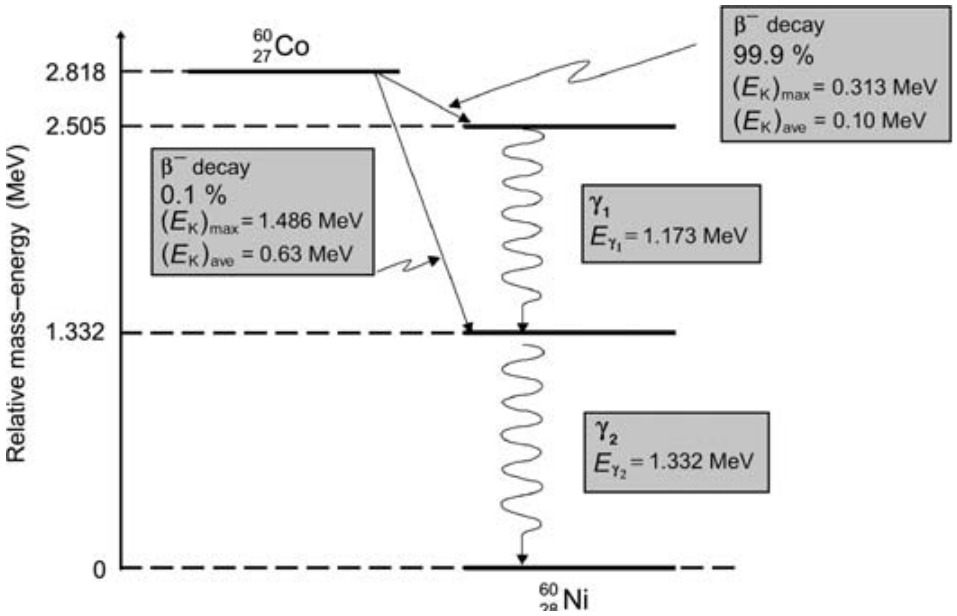

Figure 2.8: Decay process from ^{60}Co to ^{60}Ni. From [48]

For the simulations purpose the ^{60}Co spectrum of Table 3.1 was considered , taking into account that the most relevant gamma lines emitted are located at 1.33MeV and 1.17 MeV.[53]

Table 2.11: ^{60}Co spectrum.

Energy [keV]	Probability
1.17e3	99.97
1.17e3	0
1.33e3	99.99
1.33e3	0

2.8.2 50kVp χ-rays source

The photon energy spectrum used for the χ-rays were calculated using the program SpekCalc. The plot represented in Figure 2.9 is generated considering the following parameters:

- Peak voltage: 50 kVp;
- Anode material: tungsten;
- Anode angle: 20 degree;
- Filter material and thickness: aluminium, 3.9 mm and beryllium, 0.8mm.

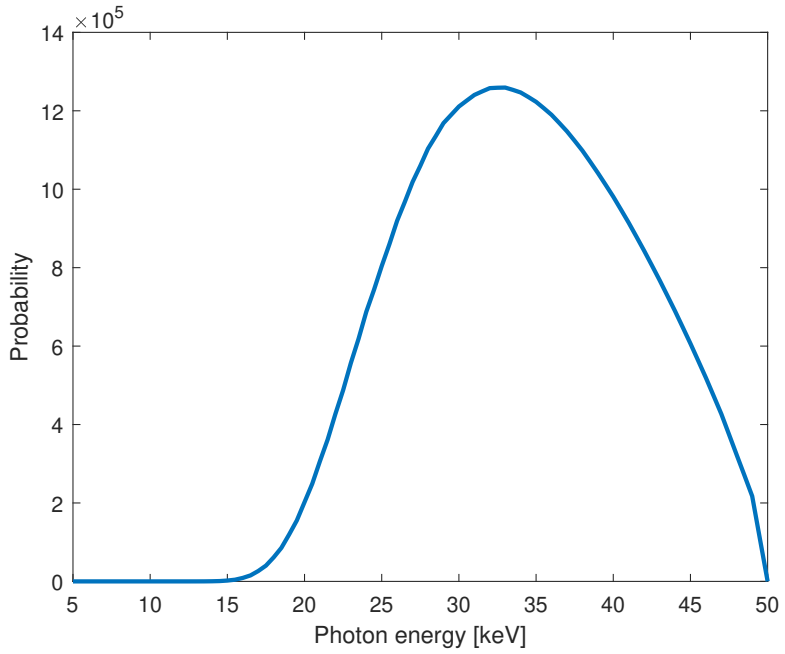

Figure 2.9: Plot of 50 kVp χ-ray spectrum used for MC simulations.

Chapter 3

Results and Discussion

This chapter reports the most relevant results obtained during the course of the work.
The validation and the computational results are presented with a discussion of the trends obtained.

3.1 Energy deposition validation results

The energy results obtained respectively for different AuNPs diameter size (d) and in the first 5 shells for an increasing radial distance of 40 µm are reported respectively in Table 3.2 and 3.1. The absolute uncertainty energy value, calculated using the Equation 2.2, was equal or lower than 1% for all AuNPs and shells.

Table 3.1: Energy deposited in each AuNP irradiated by ^{60}Co.

AuNP d [nm]	Energy [eV]
100	7.93×10^{-3}
50	3.79×10^{-3}
2	9.15×10^{-5}

Table 3.2: Energy in the first five outside shells for each AuNP size irradiated by ^{60}Co.

AuNP d [nm]	Energy shell #1 [eV]	Energy shell #2 [eV]	Energy shell #3 [eV]	Energy shell #4 [eV]	Energy shell #5 [eV]
100	10.4	29.1	45.5	59.2	71.3
50	10.3	29.0	45.5	59.2	71.3
2	10.2	29.0	45.1	59.0	70.9

These results are consistent with the Leung et al. (2011) work, showing that the energy deposited in the AuNPs is small compared to the energy deposited outside of the AuNPs that increase with the nanoparticle diameter and radially with the shells number. [30]

3.2 DEF validation results

The Dose Enhancement Factor and the associated uncertainty, calculated as described in section 2.6.2, for both χ-ray and ^{60}Co sources are presented in Table 3.3.
The results show that imposing the number of histories as parameter to stop the simulation the DEFs is affected by an high value of uncertainty, especially for the irradiation with ^{60}Co. However, the DEF obtained for the 50 kVp χ-ray for a source distance of 0.01 are consistent with the literature (see Table 3.3). In this case the results are dependent by the MC code used, cross section, and geometry setup. Also, in this work a quadratic parallel beam was chosen, whereas in the work of Li et al. a circular parallel beam was used. The DEF values decrease with the increase of the AuNP-source distance except for the 50 kVp χ-ray source and a distance of 0.1 cm. This discordance is probably due to the high uncertainty.
The DEF obtained shows a difference of one order of magnitude if using 50 kVp χ-ray instead of ^{60}Co (1 MeV). This difference can be justified considering the results presed in Figure 1.10 reporting the total mass attenuation for gold and water. In particular, it is possible to observe the difference of one order of magnitude from keV to MeV photon energy, consistently with the results obtained.
This can be also observed in the Figure 3.1 that shows the mass energy absorption coefficient (μ_{en}) and the total mass attenuation coefficient of gold as function of different photon beam energy, i.e. the coefficient decreases of one order of magnitude from 50 - 100 keV to 1 MeV.

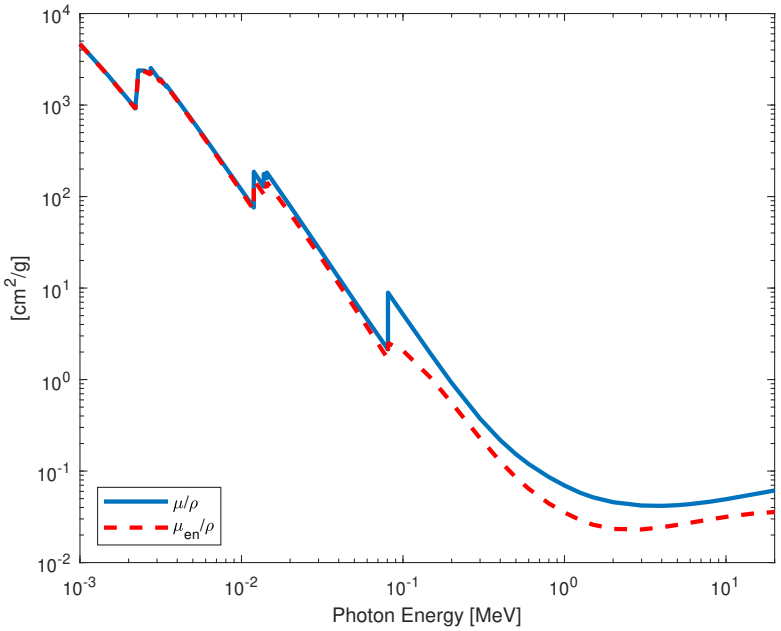

Figure 3.1: Mass attenuation and mass energy absorption coefficient in gold as function of photon energy (values taken from the NIST XCOM database) [47]

Seeing the absolute DEF uncertainty, the value of 1e-2 cm (i.e. 100 µm) is selected as the source distance for the sensitivity study for both type of sources.

Table 3.3: Dose Enhancement factor for different source distance with 50 kVp χ-ray and ^{60}Co source.

Source Distance [cm]	DEF [-] ^{60}Co	DEF [-] 50 kVp χ-ray	DEF[-] (Li et al.)	δDEF % ^{60}Co	δDEF % 50 kVp χ-ray
1e-4	2.16	77.8		45.7	9.78
1e-2	1.78	71.60	50-90*	28.8	10.2
1e-1	1.69	72.61		37.7	9.89
1	1.16	71.16		33.1	49.8

*The literature values are between 50 and 90, according to the MC code used.

3.3 Sensitivity study of beam width effect on DEF results

Considering the secondary electron equilibrium and the limitations due to the confined beam geometry the following Dose Enhancement Factor values in the first 15 shells of a single gold nanoparticle with 100 nm diameter are extrapolated in order to:

- test the computational time with increasing beam width in order to understand what is the best compromise between computational time and consistent results;
- have an idea of the overestimation of the results due to the increase of the instability of secondary charged particles;
- find the best configuration for the concentration study considering the points above described.

The results for the ^{60}Co and 50 kVp χ-ray source are shown in Figure 3.2. In particular, the sensitivity study on χ-ray highlights the non-feasibility of using a source width of 100 µm. This results from the high energy uncertainty observed in the first shell of the configuration with the water nano-particle that is over the 100% despite the number of histories simulated was higher than 2.1 $\times 10^9$.
As expected for both kind of sources, decreasing the beam size leads to the overestimation of the dose enhancement factor

- with ^{60}Co, in the first shell DEF, is observed an increase of 1.04 passing from 1µm to 150 nm source beam width;
- with 50 kVp χ-ray, in the first shell DEF, is observed an increase of 65.2 passing from 1µm to 150 nm source beam width.

Consistently with the validation the order of magnitude of difference between the irradiation with 50 kVp χ-ray source and ^{60}Co source is maintained for a source width of 1 µm.

The general shape define a DEF that decreases monotonically with the increasing of the diameter, with a maximum in the first of the 100 nm shell due to the localized effect of the AuNP. The absolute DEF uncertainties of the first water shell for each beam width are reported in Table 3.4 considered that is the one effected by the highest uncertainty.

The results show that for a number of histories between 10^8-10^9 a beam width of 150 nm is able to guarantee the lowest uncertainty for both type of sources even if this should not completely assure the secondary particle equilibrium. From these results, a beam width of

Table 3.4: Absolute DEF uncertainty in the first water shell for 50 kVp χ-ray and ^{60}Co sources for different beam width.

Source type	Beam width	δDEF % in the first water shell
^{60}Co	1 µm	30.8
	150 nm	14
50 kVp χ-ray	1 µm	8.81
	150 nm	2.93

150 nm was set as parameter for the successive concentration study. Moreover, the sensitivity analysis results on the source distance for ^{60}Co for a beam width of 150 nm with 1 cm showed in Table 3.5 highlight an average overestimation of the 0.04, that should become relevant for lower absolute DEF uncertainties.

Table 3.5: DEF results in the first 100 nm water shells irradiated by ^{60}Co and 50 kVp χ-ray for the different cell size and respectively AuNP dimension guaranteeing a constant internalization of the 30% with the respectively absolute uncertainty. Configuration 100%-0% nucleus-cytoplasm.

Source type	Source distance	Average DEF	δDEF %
^{60}Co	100 µm	1.32	14
	1 cm	1.28	14

Summing up, from this study the following parameter are chosen in order to perform the concentration study:

- 50 kVp χ-ray: beam width 150 nm, source distance 100 µm;
- ^{60}Co : beam width 150 nm, source distance 1 cm.

The chosen beam width for the two energies permits to have lower uncertainties in reasonable computational times. So, for the following concentration study, the beam width was chosen 20 nm wider than the AuNP diameter (see section 2.7.3 in Material and Methods chapter). In this way the lateral electron equilibrium is not guaranteed, but this sensitivity analysis will permit to make reasonable assessment of the DEF overestimate. The distance source-AuNPs were set different for the two energies, in order to assure longitudinal electronic equilibrium (for higher energies such as ^{60}Co, the distance higher).[21]

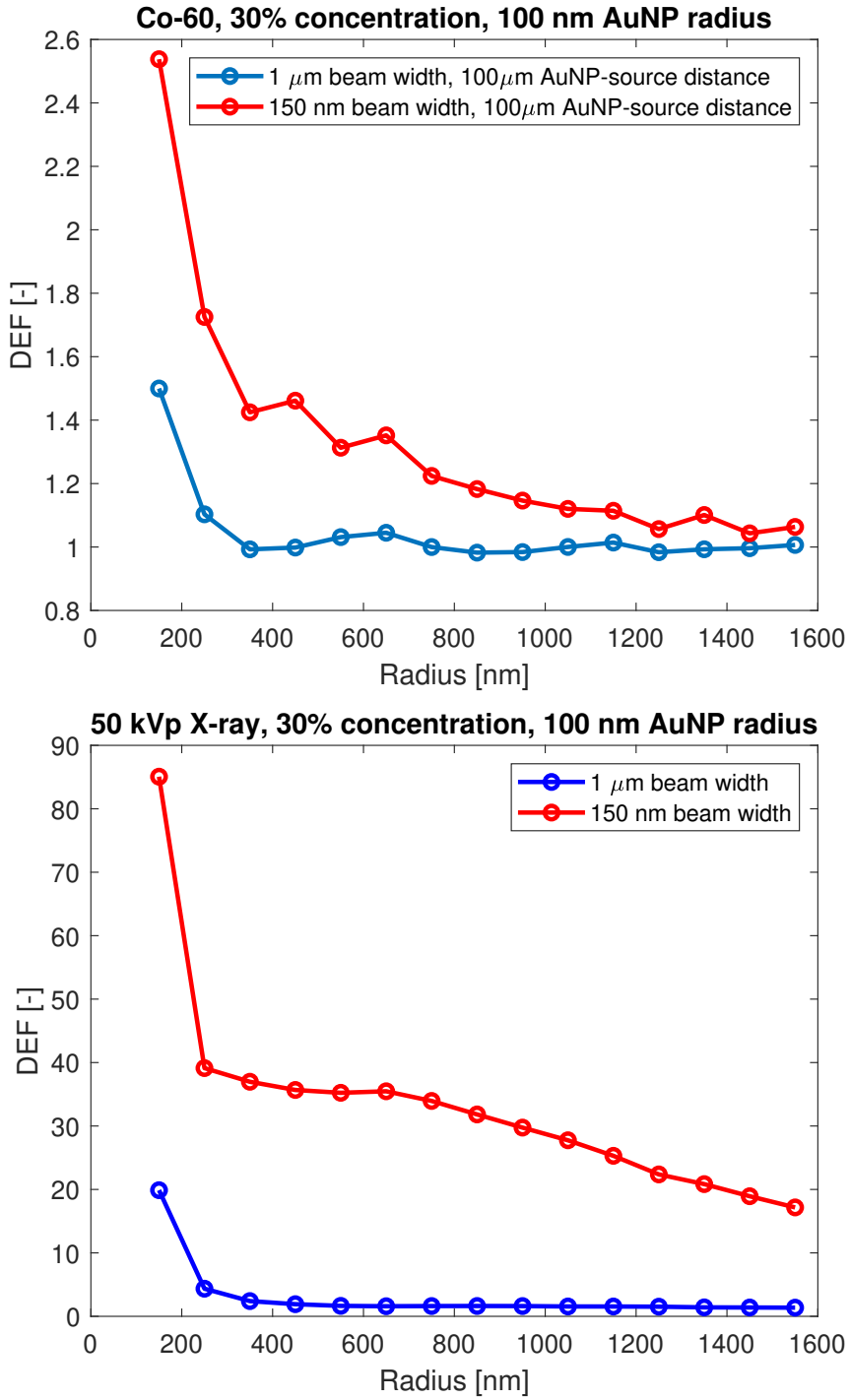

Figure 3.2: Dose Enhancement Factor plot for ^{60}Co beam sources and 50 kVp χ-ray with a constant internalization of the 30% in the nucleus and AuNP-source distance of 100 µm. The irradiation study is done considering a single gold nanoparticle of 100 nm diameter centered in the cell nucleus, surrounded by water and beam width of 150 nm and1 µm. The DEF is calculated in the first 15 shells of 100 nm around the AuNP.

3.4 Configuration 100%-0% nucleus-cytoplasm results

Figure 3.3 shows the DEFs obtained in the 30 water shell of 100 nm thickness. Like the sensitivity study, the number of histories simulated in this part was in the range of 10^8-10^9. Moreover, the simulations were stopped when the absolute energy uncertainty in the first water shell reached:

- a value $\leq$ 10% for the irradiation with ^{60}Co;
- a value $\leq$ 5% for the irradiation with 50 kVp χ-ray.

Consequently, all the uncertainties in the other water shells resulting lower than the values mentioned above. As expected, for both type of sources the average DEF increase with the AuNP diameter. The maximum value of the DEF is reached in the first water shell, then it monotonically decreases seeming to reach an asymptotic value of:

- about 1.2 for all the AuNP size irradiated with ^{60}60, after 4000 nm;
- between 50 and 100 for all the AuNP size irradiated with 550 kVp -ray source, after 4000 nm (i.e. 4 µm).

Table 3.6 reports the DEF in the first water shell with its absolute uncertainty for all AuNP size (i.e. for the different cell size analysed) and source type.

Table 3.6: DEF results in the 1st water shells, with its relative uncertainty, for ^{60}Co and 50 kVp -ray source with a source distance of 1 cm and 100 µm respectively.

Source type	Cell diameter[µm]	AuNP diameter [nm]	DEF 1st water shell	δDEF %
^{60}Co	10	372	4.79	7.2
	15	559	5.18	7.0
	25	930	4.72	7.0
	50	1862	3.48	7.1
50 kVp χ-ray	10	372	232	2.3
	15	559	284	2.6
	25	930	318	2.8
	50	1862	331	2.4

It is important to point out that the DEF in the first water shell tends to increase with the AuNP diameter for and irradiation with 50 kVp χ-ray contrarily to what happens for the irradiation with ^{60}Co. This trend can be justify considering that in the range of 50 kVp the photoelectric effect is dominant in soft tissue and (see Figure 1.6) while in the MeV range the Compton effect is the dominant one. This means that while for an irradiation with 50 kVp χ-ray the photons energy is directly absorbed from the tissue, for an irradiation with ^{60}Co the energy lost by the photons is not completely absorbed but partially dispersed in Coulomb interactions. An exception is evident in the cell with 15 µm diameter and AuNP of 930 nm where the value of the DEF in the first shell is higher than the cell with 10 µm diameter and AuNP of 559 nm, this issue could be due to the limitations on the uncertainty values effecting the results.

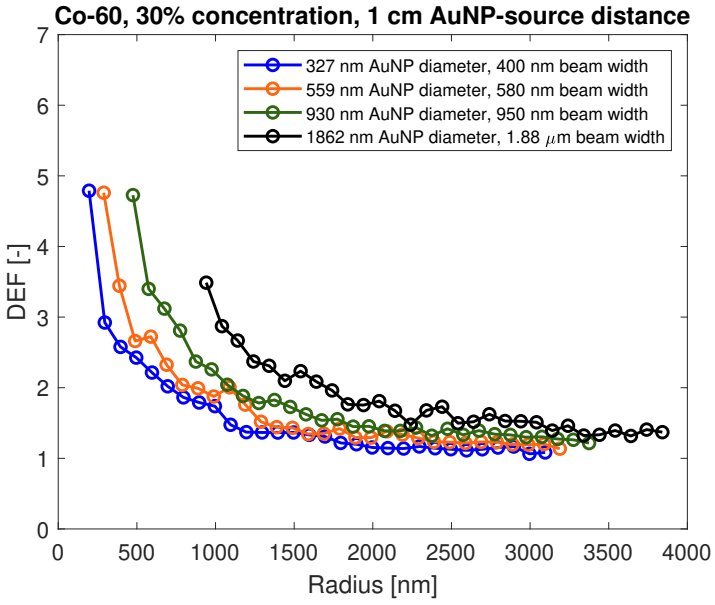

(a)

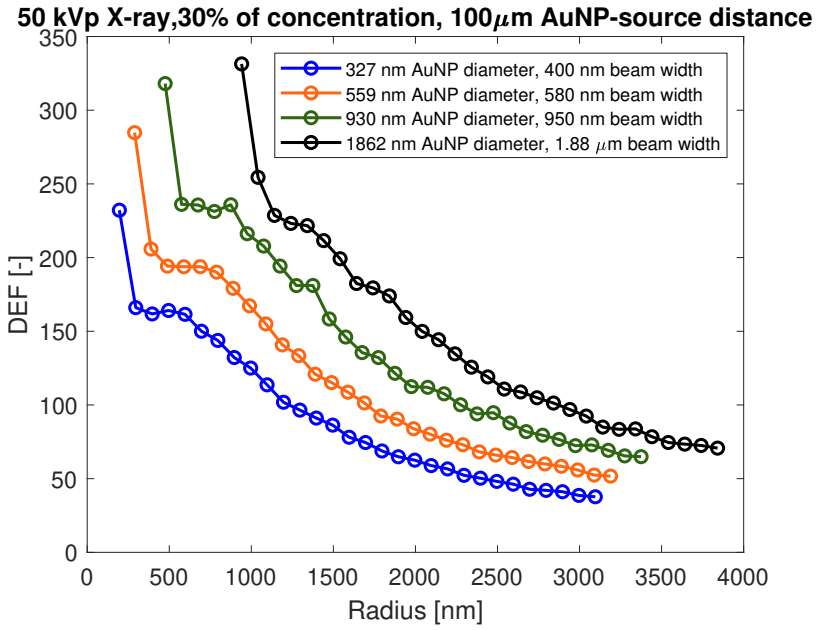

(b)

Figure 3.3: Dose Enhancement Factor plot for a) ^{60}Co and b) 50 kVp χ-ray beam source with a constant internalization of the 30% in the nucleus and an AuNP-source distance of 100 µm for different cell size. The irradiation study is done considering a single gold nanoparticle corresponding to the amount of smaller AuNPs. The AuNPs are centered in each cell nucleus, surrounded by water. The DEF is calculated in the first 30 shells of 100 nm around the AuNP.

3.5 Configuration 0%-100% nucleus-cytoplasm results

Figure 3.4 shows the DEFs obtained in 40 water shells of 100 nm thickness for ^{60}Co irradiation while in Figure 3.5 and Figure 3.6 report the DEFs detected in the same water shells with 50 kVp χ-ray irradiation. Also for this part, the number of histories simulated was in the range of 10^8-10^9. Moreover, the simulations were stopped when the absolute energy uncertainty in the shell with the lowest radius was reached:

- as low as possible for the irradiation with ^{60}Co;
- a value of $\leq$5% for the irradiation width with 50 kVp χ-ray.

Consequently, all the uncertainties in the other water shells resulting lower than the values mentioned above. The results for ^{60}Co irradiation are only referred to the first cell size of 10 µm and a beam width of 4.33 µm. This limitation is due to the fact that it is not feasible to simulate a beam with dimensions that guarantees acceptable results. This is because an higher beam width, in order to reach a low uncertainty, would need a too high computational time. The DEF shape presents some peaks, with a DEF that

- fluctuates between 1.3 and 0.8 in the nucleus;
- seems to reach an asymptotic value asymptotic value of about 1 in the cytoplasm.

The results for 50 kVp χ-ray show the maximum value of DEF reached in the two water shells with the lowest distance to the gold shells. After these two maxima the DEF rapidly decreases in the second water shell after which continues to slowly decrease seeming to reach an asymptotic value of:

- about 1.6 in the nucleus and 1.4 in the cytoplasm for the 10, 15, 25 µm diameter cell size;
- about 4.8 in the nucleus and in the cytoplasm for the 50 µm diameter cell size;

The highest DEF is reached in the nucleus. The DEF values in the nucleus and cytoplasm are in the same order of magnitude for the cell size of 10, 15 and 25 µm, while for the biggest cell size this DEF increase of one order of magnitude.
Table 3.7 and Table 3.8 report the DEF in the nearest water shells to the AuNPs cluster and the one in the water shell with the lowest radius used as parameter to stop the simulations with the respective absolute uncertainty for all cell size.

Table 3.7: DEF results in the nearest water shells to the AuNPs cluster in the nucleus and cytoplasm for ^{60}Co and 50 kVp χ-ray and source distance of 1 c and 100 µm.

Source type	Cell diameter [µm]	Au shell thickness [nm]	DEF shell nucleus	DEF shell cytoplasm
^{60}Co	10	0.463	1.09	1.01
	15	0.696	N.F	N.F.
	25	1.16	N.F	N.F.
	50	18.5	N.F.	N.F.
50 kVp	10	0.463	6.0	5.78
χ-ray	15	0.696	6.14	6.03
	25	1.16	6.53	6.38
	50	18.5	21.5	19.5

N.F.= Not feasible.

Table 3.8: DEF results in the water shells with lowest radius used as stopping parameter for the simulations with its absolute uncertainty for ^{60}Co and 50 kVp χ-ray irradiation with a source distance of 100 µm and 1 cm respectively for the configuration 0%-100% nucleus-cytoplasm for all cell size considered.

Source type	Cell diameter [µm]	Au shell thickness [nm]	DEF [-]	δDEF%
^{60}Co	10	0.463	1.30	36.8
	15	0.696	N.F.	N.F.
	25	1.16	N.F.	N.F.
	50	18.5	N.F.	N.F.
50 kVp	10	0.463	1.49	3.2
χ-ray	15	0.696	1.52	4.1
	25	1.16	1.58	2.3
	50	18.5	4.07	2.5

All the cell sizes highlight an higher DEF in the nucleus respect to the cytoplasm in the first 100 nm far from the AuNPs cluster for both source type. For the ^{60}Co irradiation, the peaks in the cytoplasm region (Figure 3.4) are due to the limitation related to the high uncertainty of the DEF in the shell used as stopping parameter.

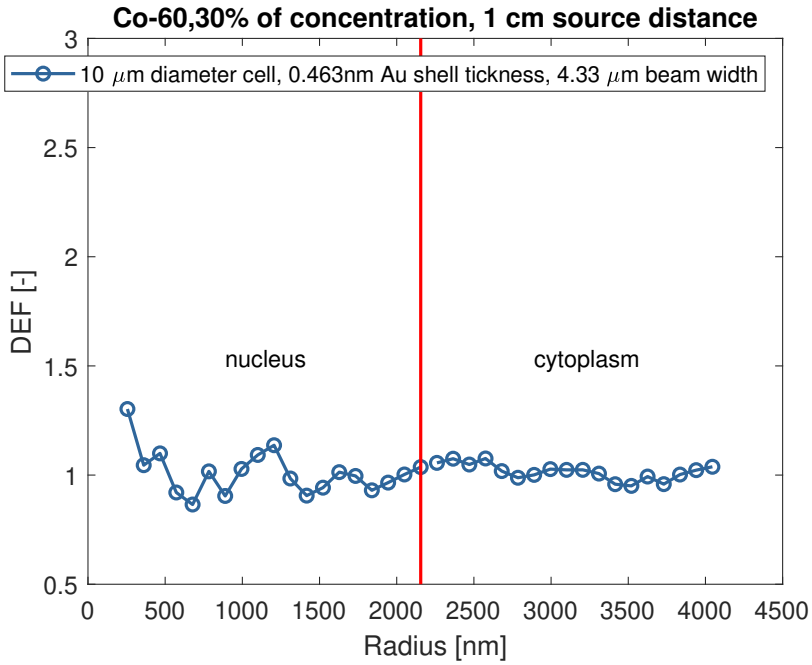

Figure 3.4: Dose Enhancement Factor plot for ^{60}Co beam source with a constant internalization of the 30% detected in 20 water shell with 100 nm thickness in the nucleus and in the cytoplasm and a source distance of 1 cm from the center of the cell for cell diameter 10µm. The irradiation study is done considering a gold shell corresponding to the amount of smaller AuNPs calculated in section 2.7.2. The gold shell are located in the cytoplasm close to the nuclear membrane.)

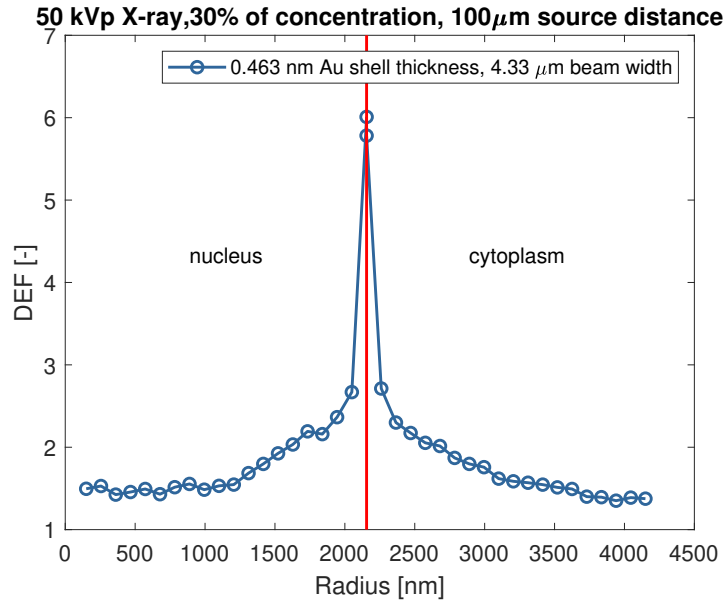

(a)

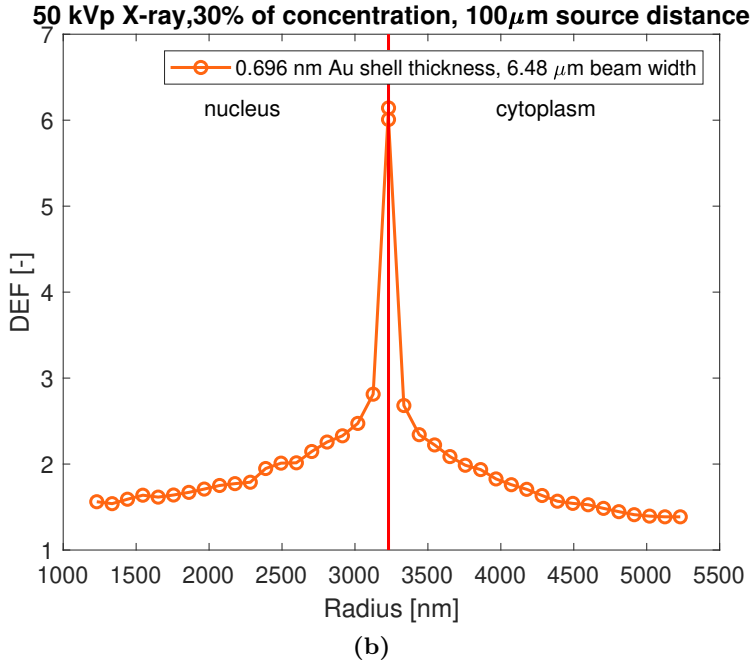

(b)

Figure 3.5: Dose Enhancement Factor plot for 50 kVp χ-ray beam source with a constant internalization of the 30% detected in 20 water shell in the nucleus and in the cytoplasm with 100 nm thickness and source distance of 100 µm from the center of the cell for a) cell diameter 10 µm and b) cell diameter 15 µm. The irradiation study is done considering a gold shell corresponding to the amount of smaller AuNPs. The gold shell are located in the cytoplasm close to the nuclear membrane.

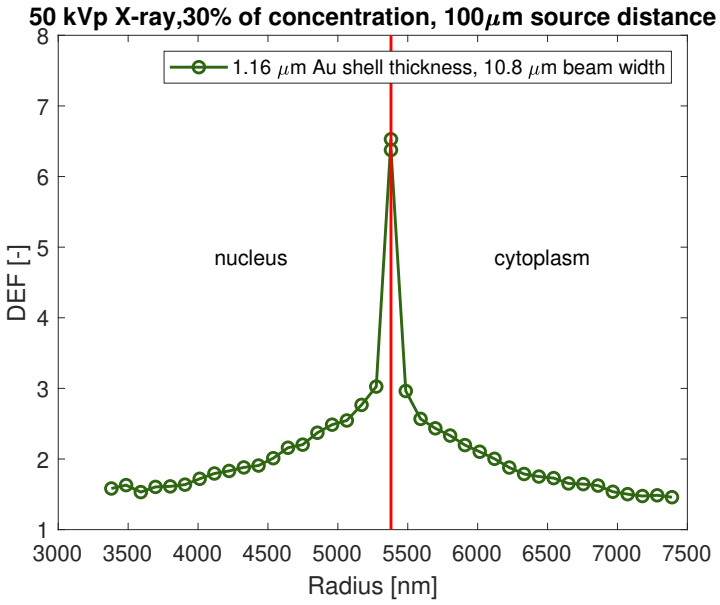

(a)

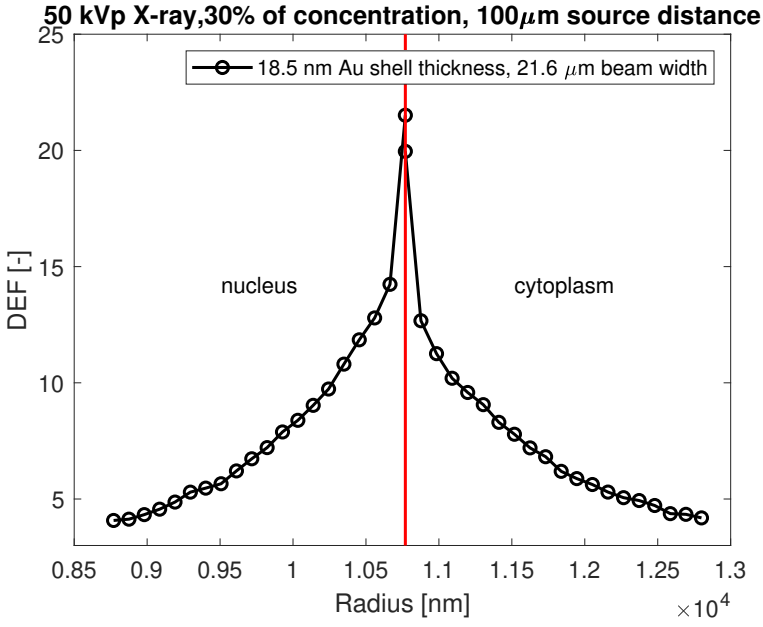

(b)

Figure 3.6: Dose Enhancement Factor plot for 50 kVp χ-ray beam source with a constant internalization of the 30% detected in 20 water shell in the nucleus and in the cytoplasm with 100 nm thickness and source distance of 100 µm from the center of the cell for a) cell diameter 25 µm and b) cell diameter 50 µm. The irradiation study is done considering a gold shell corresponding to the amount of smaller AuNPs. The gold shell are located in the cytoplasm close to the nuclear membrane.

Chapter 4

Conclusions and future improvements

In this study the Dose Enhancement Effect due to the presence gold nanoparticle in the gliobastoma cells was evaluated for energy spectrum of 50 keV χ-ray and 1 MeV ^{60}Co. The analysis was done firstly to qualitatively compare the computational results with the experimental data of an irradiation with ^{60}Co, then in order to maximize the DEF the 50 kVp χ-ray spectrum was tested considering different configurations involving different AuNP concentration and localization. The conclusion is drawn in order to evaluate the optimal configuration, between a localized concentration in the nucleus or in the cytoplasm of the cell, taking into account the physical results combined with possible biological effects.

4.1 Comparison between the two configurations: ^{60}Co irradiation

In order to compare the two different configurations with a concentration 100%-0% and 0%-100% nucleus-cytoplasm with the aim to understand what is the best configurations and the best concentration assuring the maximum DEF, the mean value of the Dose Enhancement factor in the first 2 µm in the nucleus cell for each configuration and each cell size is calculated. This DEF value is the result of two averaging processes: firstly, it has been computed the average value between different concentrations of the same cell type; then, the average of these outcomes has been derived. This is representative for all the analyzed cases and allows an immediately comparison. (Table 4.1) While, for the comparison between the cell sizes the concentration that maximizes the DEF is obtained by considering directly the mean value of the DEF in the first 2 µm from the nucleus for the 100%-0% and in the 0%-100% nucleus-cytoplasm configuration. (Table 4.2)

This comparisons denotes that the highest DEF in the first 2 µm of the cell could be achieved in a cell size of 50 µm diameter with a cluster of 8.18×10^7 AuNPs, corresponding to the 30%of internalization, if they are entirely located in the nucleus. However, if the effect to consider is DEF in the first nanometer a cluster of 6.54×10^6 guarantee the highest Dose Enhancement. Moreover, a comparison between the 0%-100% configuration is not possible due to the limitations of the simulations(see Section Results and Discussion chapters 3.4 and 3.5). However from the results we have it is possible to expect a conclusion similar to the 50 kVp χ-ray irradiation with an highest average DEF in the highest cell size due to the highest

Table 4.1: Average DEF results in the first 2 µm far from the AuNPs clusters in the nucleus, for the concentration configuration 0%-100% and 100%-0% nucleus-cytoplasm irradiated by ^{60}Co.

Source type	Configuration	$\overline{\text{DEF}}$between the cell [-]
^{60}Co	100%-0% nucleus-cytoplasm	1.96
^{60}Co	0%-100% nucleus-cytoplasm	*1.01

*Value corresponding to the cell diameter of 10 µm (see Section Results and Discussion, chapter 3.5).

Table 4.2: Average DEF results in the first 2 µm far from the AuNPs clusters in the nucleus, for the concentration configuration 0%-100% and 100%-0% nucleus-cytoplasm irradiated by ^{60}Co. For detailed DEF trend in each shell see Figure 3.3 and Figure 3.4.

Source type	Configuration	Beam Width	Cell diameter thickness[µm]	$\overline{\text{DEF}}$ [-]
^{60}Co	100%-0% nucleus-cytoplasm	+20 nm respect to the external gold shell diameter	10	1.83
			15	1.97
			25	2.00
			50	**2.05**
^{60}Co	0%-100% nucleus-cytoplasm	+20 nm respect to the external gold shell diameter	10	1.01
			15	N.F.
			25	N.F.
			50	N.F.

number of AuNPs.

4.2 Comparison between the two configurations: 50 kVp χ-ray

The DEF study with the spectra of 50 kVp generated by the χ-ray was introduced with the aim to maximise the DEF considering not only the ^{60}Co but an energy spectrum that guarantee an higher mass attenuation coefficient with an enhancement of the photoelectric effect and the inner shell ionization. In this regard, in the range of 50-100 kVp the gold present a photoelectric cross-section higher than in the MeV energy (i.e. the range of ^{60}Co spectrum, Figure 1.10). This means that the range of the generated secondary electrons is higher, consequently the deposited energy is higher and more localized (in the nanometer and micrometer range) with respect to the MeV energy, as is also confirmed from the Figures 1.10 and 1.11. To compare the two different configurations with a concentration 100%-0% and 0%-100% nucleus-cytoplasm and understand what is the best configurations and the best concentration assuring the maximum DEF, the mean value of the Dose Enhancement factor in the first 2 µm in the nucleus cell for each configuration and each cell size was calculated. Then, an average value for each concentration configuration is obtained. (Table 4.3)
While, for the comparison between the cell size the concentration maximizing the DEF is obtained considered directly the mean value of the DEF in the first 2 µm in the nucleus for the configuration 100%-0% nucleus-cytoplasm and in the 2 µm surrounding the AuNP cluster for the configuration 0%-100%. (Table 4.4)

Table 4.3: Average DEF results in the first 2 µm far from the AuNPs clusters in the nucleus, for the concentration configuration 0%-100% and 100%-0% nucleus-cytoplasm irradiated by 50 kVp -ray.

Source type	Configuration	$\overline{\text{DEF}}$between the cell [-]
50 kVp χ-ray	100%-0% nuceus-cytoplasm	**152**
50 kVp χ-ray	0%-100% nuceus-cytoplasm	3.51

This comparisons denotes that the highest average DEF in the first 2µm surrounding the AuNPs cluster can be generally achieved with the configuration 100%-0% nucleus-cytoplasm. Whereas, comparing the average DEF in each cell and concentration configuration, the highest DEF in the first 2 µm surrounding the Au shell is reached in a cell size of 50 µm diameter with a cluster of 8.18×10^7 AuNPs, corresponding to the 30% of internalization, for both concentration configurations.

Table 4.4: Average DEF results in the first 2 µm far from the AuNPs clusters in the nucleus and in the 2µm surrounding the Au shell for the concentration configuration 0%-100% and 100%-0% nucleus-cytoplasm irradiated by 50 kVp -ray. For detailed DEF trend in each shell see Figure 3.3 and Figure 3.4.

Source type	Configuration	Beam width	Cell diameter thickness [µm]	$\overline{DEF}$ [-]
50 kVp	100%-0%	+20 nm	10	117
χ-ray	nucleus-cytoplasm	respect to the	15	145
		external gold shell	25	172
		diameter	50	**173**
50 kVp	0%-100%	+20 nm	10	1.95
χ-ray	nucleus-cytoplasm	respect to the	15	2.05
		external gold shell	25	2.17
		diameter	50	**7.71**

4.3 Optimal configuration

The obtained results can lead to an evaluation of which is the optimal configuration considering a cluster of AuNPs located in the nucleus or cytoplasm. As demonstrate above, the presence of a cluster of AuNPs increase the dose delivered to the cell this means that efficiency of radiotherapy can be increased. This efficiency increase results in the improvement of the tumor control probability and the decrease of the normal tissue complication probability because a lower delivered dose is necessary to kill a certain amount of cells in presence of the AuNPs a low dose delivered is necessary. Consequently, it is possible to operate in large therapeutic window minimizing the side effect on the healthy cells. The death of a cancer cells can be due to a direct damage to DNA, with a formation of strand breaks (SSBs or DSBs), or an indirect rupture of molecular bonds and oxidation of DNA due to reactive oxygen species. In this context, if the AuNPs are used to enhance the DNA damage and they are localized next to the DNA, the configuration with the AuNP cluster in the nucleus can be considered as the one fitting the aim, resulting also in the highest DEF at the micrometer ranges. However,in reality, a good internalization does not guarantee an homogeneous distribution in the cell nucleus: the nuclear membrane can be seen as an additional barrier for the AuNP to overcome. On the other hand, the results obtained with a AuNP concentration in the cytoplasm next to the nuclear membrane highlights the possibility to obtain, for 50 kVp χ-ray two peak of DEF near the surface of AuNP in the 100 nm range with a lower dose enhance reached in the micrometer range. These two peaks are almost the same and located in both nucleus and cytoplasm, this means that if from one side it is possible to reach the DNA as target in the nucleus, on the other side in the cytoplasm the mitochondrial DNA that generates ROS indirectly target the nuclear DNA. However, the DEF obtained in the configuration 0%-100% nucleus-cytoplasm is lower than a cluster of AuNPs located in the nucleus, this seems closer to the reality and guarantee a double effects that experiments could confirm. Finally, considering the physics related to the total gold mass attenuation coefficient for the two spectra used, a source energy of 50 kVp guarantee an higher photoelectric effects respect to the 1 MeV, i.e. the highest DEF. However is not possible to predict a priori what

is the best energy source that can be different considering the dose rate and the biological effects obtained. Specifically, the enhancement factor could strongly depend on the cell biology, internalization percentage, DNA damage type (with consequent reparation mechanisms that could depend also by the irradiation rate) and megavoltage energies could add additional processes in the radiosensitising effect of AuNPs.

4.4 Future Improvements

The firs improvement on the model used could be an improvements on the geometry configuration such as:

- modeling the AuNPs with different shapes, such as rod, disk, full hollow;
- considering the SP peptide impacting the dose enhancement.

Secondly, the simulations of more cluster configurations in order to have a wide view of the effect on the dose enhance with different distributions considering, also a sparse localization. Then, considering the importance of the photoelectric effect in Au in the range 50-100 kV, energy spectra between these two values can be considered in order to find what this the one who physical maximise the DEF in a larger energy range. Finally, experiments and radiobiological models could be implemented in order to qualitative correlate the simulation results with real irradiation effects on the gliobastoma cell line and evaluate the mechanisms of cell death and the clonogenic assay.

Bibliography

[1] C. Vens A. C. Begg, F. A. Stewart. Strategies to improve radiotherapy with targeted drugs. *Nature Reviews Cancer*, 11(4), 2011.

[2] Z. Abbas and S. Rehman. Neoplasm: An overview of cancer treatment modalities. *Hafiz Naveed Shahzad*, page 139, 2018.

[3] American Brain Tumor Association. Gliobastoma (gbm). "https://www.abta.org/tumor_types/glioblastoma-gbm/.

[4] J. C. Borbinha. *Organ Dose Estimates in Thorax CT: Voxel Phantom Organ Matching With Individual Patient Anatomy.* PhD Thesis, 2017.

[5] David J. Brenner. The linear-quadratic model is an appropriate methodology for determining isoeffective doses at large doses per fraction. *Seminars in radiation oncology*, 18(4):234–239, 2008.

[6] W. J. Gullick C. R. Lewanski. *Radiotherapy and cellular signalling.* Lancet Oncology, 2001.

[7] G. Casella C. Robert. A short history of markov chain monte carlo: Subjective recollections from incomplete data. *Statistical Science*, pages 102–115, 2011.

[8] M. Dougan and G. Dranoff. Immune therapy for cancer. *Annual review of immunology*, 2009.

[9] A. J. Giacca E. J. Hall. *Radiobiology for the Radiologist*, volume eight edition. 2006.

[10] A. Kling et al. *Advanced Monte Carlo for Radiation Physics, Particle Transport Simulation and Applications: Proceedings of the Monte Carlo 2000 Conference, Lisbon, 23–26 October 2000.* Springer Science Business Media, 2014.

[11] A. Majkowka-Pilip et al. Application of neurokinin-1 receptor in targeted strategies for glioma treatment. part i: Synthesis and evaluation of substance p fragments labeled with 99mtc and 177lu as potential receptor radiopharmaceuticals. *Molecules*, 23(10):2542, 2018.

[12] A. Malik et al. Role of natural radiosensitizers and cancer cell radioresistance: an update. *Analytical Cellular Pathology, Hindawi Publishing Corporation*, 2016.

[13] A. Von Deimling et al. Association of epidermal growth factor receptor gene amplification with loss of chromosome 10 in human glioblastoma multiforme. *Journal of neurosurgery*, 1992.

[14] B. Rajamanickam et al. Cancer and radiation therapy: current advances and future directions. *International Journal of Medical Sciences*, 9(3):193–199, 2012.

[15] D. Y. Joh et al. Selective targeting of brain tumors with gold nanoparticle-induced radiosensitization. *Plos one*, 8(4), 2013.

[16] D.N. Louis et al. The 2016 world health organization classification of tumors of the central nervous system: a summary. *Acta neuropathologica*, 2016.

[17] D.Selzer et al. Finite and infinite dosing: difficulties in measurements, evaluations and predictions. *Advanced drug delivery reviews*, 65(2):278–294, 2013.

[18] F. Kazmi et al. Megavoltage radiosensitization of gold nanoparticles on a glioblastoma cancer cell line using a clinical platform. *International Journal of Molecular Sciences*, 21(2):429, 2020.

[19] F. Salvat et al. *PENELOPE-2018: A Code System for Monte Carlo Simulation of Electron and Photon Transport A Code System for Monte Carlo. Barcelona, Spain: OECD/NEA*. Barcelona, Spain: OECD/NEA, 2018.

[20] F. Silva et al. Interrogating the role of receptor-mediated mechanisms: biological fate of peptide-functionalized radiolabeled gold nanoparticles in tumor mice. *Bioconjugate chemistry*, 27(4):1153–1164, 2016.

[21] H. Rabus et al. Determining dose enhancement factors of high-z nanoparticles from simulations where lateral secondary particle disequilibrium exists. *Physics in Medicine Biology*, 64(15), 2019.

[22] H. Wang et al. Cancer radiosensitizers. *Trends in pharmacological sciences*, 39(1):24–48, 2018.

[23] J. C. Adams et al. *The Fortran 2003 handbook: the complete syntax, features and procedures*. 2008.

[24] J. S. Bell et al. Global incidence of brain and spinal tumors by geographic region and income level based on cancer registry data. *Journal of Clinical Neuroscience*, 66:121–127, 2019.

[25] K. T. Butterwoth et al. Physical basis and biological mechanisms of gold nanoparticle radiosensitization. *Nanoscale*, 4(16):4830–4838, 2012.

[26] KH. Kalan et al. Brain cancer in the world: An epidemiological review. *World Cancer Research Journal*, 2019.

[27] L. Bobyk et al. Photoactivation of gold nanoparticles for glioma treatment. *Nanomedicine: Nanotechnology, Biology and Medicine*, 9(7):1089–1097, 2013.

[28] L. Cui et al. Radiosensitization by gold nanoparticles: Will they ever make it to the clinic? *Radiotherapy and Oncology*, 124(3):344–356, 2017.

[29] L. Taggart et al. The role of mitochondrial function in gold nanoparticle mediated radiosensitisation. *Cancer nanotechnology*, 5(1):1–12, 2014.

[30] M. K. K. Leung et al. Irradiation of gold nanoparticles by x-rays: Monte carlo simulation of dose enhancements and the spatial properties of the secondary electrons production. *Medical physics*, 38(2):624–631, 2011.

[31] N. K. Kaushik et al. Altered antioxidant system stimulates dielectric barrier discharge plasma-induced cell death for solid tumor cell treatment. *PloS one*, 9(7), 2014.

[32] R. S. Bindra et al. Gbm radiosensitizers: dead in the water... or just the beginning? *Journal of neuro-oncology*, 134(3):513–521, 2017.

[33] S. David et al. *Basic radiotherapy physics and biology*. Springer International Publishing, 2014.

[34] S. Rockwell et al. Hypoxia and radiation therapy: past history, ongoing research, and future promise. *Current molecular medicine*, 9(3):445–458, 2009.

[35] W. B. Li et al. Intercomparison of dose enhancement ratio and secondary electron spectra for gold nanoparticles irradiated by x-rays calculated using multiple monte carlo simulation codes. *Physica Medica*, 69:147–163, 2020.

[36] WORLD HEALTH ORGANIZATION et al. *World health statistics 2019: monitoring health for the SDGs, sustainable development goals*. 2019.

[37] Y. Liu et al. Metal-based nanoenhancers for future radiotherapy: radiosensitizing and synergistic effects on tumor cells. *Theranostics*, 8(7):1824, 2018.

[38] U. Fantz. Dose and volume specification for reporting intracavitary therapy in gynecology: Report 38. *Journal of the ICRU*, 14(2), 2014.

[39] The National Centre for Stereotactic Radiosurgery. Nhs sheffield teaching hospitals. "http://www.gammaknife.org.uk/.

[40] Equicare Healt. Exploration of non-systemic cancer treatment modalities. "https://equicarehealth.com/exploration-of-non-systemic-cancer-treatment-modalities/.

[41] M. D. Huber and L. Gerace. The size-wise nucleus: nuclear volume control in eukaryotes. *The Journal of cell biology*, 179(4):283–584, 2007.

[42] National Cancer Institute. Types of Cancer Treatments. https://www.cancer.gov/about-cancer/treatment/types.

[43] E. Lechtman. *A Monte Carlo-based model of gold nanoparticle radiosensitization*. University of Toronto, 2013.

[44] A. Van der Kogel M. C. Joiner. *Basic clinical radiobiology fourth edition*. Hodder Arnold, 2009.

[45] C. Mendes. *Multifunctional Gold Nanoparticles for Chemoradiotherapy of Glioblastoma*. 2020.

[46] R. L. Murray and K. E.Holbert. *Nuclear Energy an Introduction to the Concepts, Systems, and Applications of Nuclear Processes*, volume 5. Elsevier, seventh edition, 2014.

[47] NIST. Element/compound/mixture selection - nist.

[48] E. B. Podgoorsak. *Radiation physics for medical physicists.* Springer, 2006.

[49] R. W. Ruddon. *Cancer biology.* Oxford University Prss, 2007.

[50] WC. RÖNTGEN. *On a new kind of rays.* Science, 1896.

[51] s. D. Perrault et al. Mediating tumor targeting efficiency of nanoparticles through design. *Nano letters*, 9(5):1909–1915, 2009.

[52] H. K. W. Law S. Y. Tam, V. W. C. Wu. Influence of autophagy on the efficacy of radiotherapy. *Journal of the ICRU*, 12(57), 2017.

[53] J. Sempau. *PENELOPE/penEasy User Manual, Version 2019-01-01.*

[54] A. Sudhakar. History of cancer, ancient and modern treatment methods. 2009.

[55] Mayo Clinic website. Diseases conditions: Gliobastoma. "https://www.mayoclinic.org/diseases-conditions/glioblastoma/cdc-20350148,.

[56] S. Lacombe Z. Kuncic. Nanoparticle radio-enhancement: principles, progress and application to cancer treatment. *Physics in Medicine Biology*, 63(2), 2018.

[57] P. Zygmanski and E. Sajo. Nanoscale radiation transport and clinical beam modeling for gold nanoparticle dose enhanced radiotherapy (gnpt) using x-rays. *The British journal of radiology*, 2016.